A Spontaneous Mutation in *kdsD*, a Biosynthesis Gene for 3-Deoxy-$_{D}$-*manno*-Octulosonic Acid, Occurred in a Ciprofloxacin Resistant Strain of *Francisella tularensis* and Causes a High Level of Attenuation in Murine Models of Tularemia

Taylor Chance[1*]; Jennifer Chua[2]; Ronald G. Toothman[2]; Jason T. Ladner[3]; Jonathan E. Nuss[4]; Jo Lynn Raymond[1]; Fabrice V. Biot[5]; Samandra Demons[2]; Lynda Miller[2]; Sherry Mou[2]; Galina Koroleva[3], Sean Lovett[3]; Gustavo Palacios[3]; Nicholas Vietri[2]; Patricia Worsham[2], Christopher Cote[2]; Todd Kijek[4]; and Joel A. Bozue[2**]

Pathology Division[1]; Bacteriology Division[2]; Center for Genome Sciences[3]; Department of Molecular and Translational Sciences[4]; the United States Army of Medical Research Institute of Infectious Diseases; Fort Detrick, MD 21702

Institut de Recherche Biomédicale des Armées, Département de Biologie des Agents Transmissibles, Unité de Bactériologie/UMR_MD1, B.P. 73, F-91220 Brétigny-sur-Orge, France[5]

*Current address:Veterinary Pathology Services, Joint Pathology Center, Silver Spring, MD 20910

** Corresponding author: joel.a.bozue.civ@mail.mil

Short title: A Ciprofloxacin Resistant Strain of *F. tularensis* Is Highly Attenuated

Abstract (300 words)

Francisella tularensis is a gram–negative facultative intracellular bacterial pathogen that can infect many mammalian species, including humans. Because of its ability to cause a lethal infection, low infectious dose, and aerosolizable nature, *F. tularensis* subspecies *tularensis* is considered a potential biowarfare agent. Due to its in vitro efficacy, ciprofloxacin is one of the antibiotics recommended for post-exposure prophylaxis of tularemia. In order to identify therapeutics that will be efficacious against infections caused by drug resistant select-agents and to better understand the threat, we sought to characterize an existing ciprofloxacin resistant (CipR) mutant in the Schu S4 strain of *F. tularensis* by determining its phenotypic characteristics and sequencing the chromosome to determine additional genetic alterations that occurred during the selection process. The sequence of the CipR strain showed additional mutations which likely occurred spontaneously during the selection process. Of particular interest was a frameshift mutation within *kdsD* which encodes for an enzyme necessary for the production of 3-Deoxy-$_D$-*manno*-Octulosonic Acid (KDO), an integral component of the lipopolysaccharide (LPS). A *kdsD* mutant was constructed in the Schu S4 strain. Although it was not resistant to ciprofloxacin, it shared many phenotypic characteristics with the CipR strain, including growth defects under different conditions, sensitivity to hydrophobic agents, altered LPS profiles, and severe attenuation in multiple models of murine tularemia. This study demonstrates that the KdsD enzyme is an attractive therapeutic target for developing novel medical countermeasures.

Author Summary (150-200 words nontechnical) :

Francisella tularensis causes the life threatening disease tularemia that can be transmitted to humans, the most common of which is from an infected insect bite. It is considered a biowarfare agent because it is aerosolizable and has a low infectious dose. Additional threats can result from naturally occurring or intentionally generated antibiotic resistant strains. In studying a ciprofloxacin resistant strain of *F. tularensis*, it was found to contain many mutations, including in the gene, *kdsD*. KdsD is responsible for synthesizing a part of the *Francisella* lipopolysaccharide, a component found on the surface of the bacteria. We demonstrate that a functional KdsD enzyme is necessary for growth, survival within macrophages, and the ability to cause disease in mice. These results suggest that KdsD could be targeted for drug development as a new antibiotic.

Introduction:

Francisella tularensis is a gram-negative bacterium that causes the life threatening and debilitating disease tularemia. As a facultative intracellular pathogen, its ability to replicate within various host cells, such as macrophages, dendritic cells, neutrophils, and epithelial cells is well documented and essential for virulence (1-11). *F. tularensis* is able to infect a wide range of animal species, including humans. *F. tularensis* can be transmitted to humans through a number of routes; the most common being the bite of an infected insect or other arthropod vector (12-15). Human illness can range from the ulceroglandular form to more serious pneumonic or typhoidal tularemia (13). In pneumonic tularemia, infection progresses from the lungs to other organs, mainly the liver and spleen (16-21). The risk of infection is associated mainly with two subspecies, the more virulent *F. tularensis* ssp. *tularensis* (type A) and the less virulent *F. tularensis* ssp. *holarctica* (type B). .

The infective dose of *F. tularensis* to a human by either subcutaneous or inhalation delivery is extremely low (18, 22). Due to its highly pathogenic and aerosizable nature, *F. tularensis* is classified by the US Department of Health and Human Services as a Tier 1 Select Agent. Based upon these characteristics, *F. tularensis* poses a serious potential threat for use as a biological weapon and has been previously developed as such (16, 23). This threat is of even greater concern with the existence of antibiotic resistant strains of *Francisella* which has previously been demonstrated (24-26).

One of the major virulence factors of *Francisella* is lipopolysaccharide (LPS) which plays an important role in evasion of the host immune responses (27-31). LPS is the major outer surface structure of gram-negative bacteria and consists of three components: lipid A, a glucosamine-based glycolipid; an eight carbon sugar, 3-Deoxy-$_{D}$-*manno*-Octulosonic Acid

(KDO); and the O-antigen polysaccharide (32). The endotoxin of *F. tularensis* does not bind to the LPS binding protein and does not activate the TLR4 signaling pathway (33, 34). In contrast, lipid A moieties from other gram-negative bacteria are able to interact with the Toll-like-receptor 4, activating the innate immune system to stimulate a strong proinflammatory response (28, 34-36). The inertness of *F. tularensis* LPS is speculated to be due to the atypical lipid A structure that is distinct from other gram-negative bacteria. Specifically, *F. tularensis* lipid A is asymmetrical and tetraacylated, possesses longer length of fatty acid chains, lacks phosphate substituents, and contains a unique amino sugar moiety (27, 29, 32, 37-40). .

The traditional therapy for tularemia is streptomycin, tetracycline, or doxycycline (17, 41-44). However, the fluorinated quinolone, ciprofloxacin, may offer advantages as a first-line therapy of treatment of tularemia and is recommended as an acceptable treatment option for *F. tularensis*, particularly after an aerosol exposure resulting from the use as a biological weapon (16, 45-51). The advantages for the use of ciprofloxacin over other antibiotics are the bactericidal effects, the potential for oral administration, and demonstrated in vitro activity (43, 52, 53). Ciprofloxacin targets the bacterial type II enzymes, DNA gyrase (GyrA and GyrB) and topoisomerase IV (ParC and ParE) (54, 55) and functions by stabilizing an intermediate stage of the DNA replication reaction thus inhibiting cell division (56-58). Resistance to ciprofloxacin is caused by changes to the amino acid sequences around the enzyme active site resulting in reduced drug affinity and continued gyrase/topoisomerase activity thereby allowing for continued bacterial cell growth. Quinolone resistance-determining region of *gyrA*, *gyrB*, *parC*, and *parE* genes, which are genetic hotspots within the bacterial genome, give rise to mutations that cause ciprofloxacin resistance by altering key amino acid residues in the topoisomerase II enzymes (57, 59).

In a previous study, a *F. tularensis* ciprofloxacin resistant (CipR) mutant of Schu S4 was generated by serially passaging on increasing concentrations of the antibiotic (24). The CipR mutant contained two non-synonymous substitutions in *gyrA* and a five bp deletion in *gyrA*. In the current study, we further characterized the phenotype of the Schu S4 CipR strain and more importantly determined if this strain retained virulence in animal models of tularemia. The genome was sequenced for identifying other genetic alterations which occurred during the selection process, excluding those previously described to *gyrA* and *parE*. Interestingly, one of the other mutations to the CipR strain was a frameshift in the *kdsD* gene which encodes for $_{D}$-arabinose 5-phosphate isomerase. KdsD is an enzyme that catalyzes the conversion of the pentose pathway intermediate $_{D}$-ribulose 5-phosphate (R5P) into D-arabinose 5-phosphate (A5P) (60). A5P is a precursor of KDO, an integral part of the LPS, in which the lipid A-KDO molecule serves as a linker for the O-antigen polysaccharide (36). As LPS is known to be an important virulence factor for *F. tularensis* (61-66), we sought to determine if the mutation of the *kdsD* gene led to many of the characteristics observed for the CipR strain, such as the lack of an O-antigen and loss of virulence in various murine models of tularemia. We found that many of the phentoytpes observed with the kdsD mutant similar to those of CipR.

Results:

The genome of the CipR strain was sequenced and additional mutations were identified.

The CipR strain was previously examined for mutations to genes that comprise the quinolone resistance-determining region which frequently give rise to ciprofloxacin resistance (57, 59). From the study by Loveless et al. (24), the CipR strain was shown to contain two non-synonymous substitutions in *gyrA* and a five bp deletion in *gyrA*. To determine if other relevant

mutations had occurred during in vitro passaging for selection of ciprofloxacin resistance, the genome of the CipR strain was sequenced (Genbank: NC_006570). This resulted in 113,394 polymerase reads with an average read length of 6,626 bp (126,205 subreads, avg. length of 5935 bp). The genome assembled into a single contig of 1,877,832 bp with 1787 CDS features, 10 rRNA genes and 38 tRNA genes (GenBank: CP013853). The assembly contained a single gap in the middle of one copy of the *Francisella* pathogenicity island (67). This region is ~30 kb and nearly perfectly duplicated in *F. tularensis* Schu S4; therefore, it is impossible to assemble across this region with the read lengths in the obtained dataset.

From this analysis, eight additional mutations to the CipR chromosome were identified within seven different genes (Table 2), and we verified the previously described alterations to *gyrA* and *parE*. Most of the mutations were base pair changes leading to an amino acid substitution for *fabH*, *fabF*, *FTT_0807*, *FTT_0676*, and *FTT_1573*. The *fupA* gene experienced a base pair deletion at nucleotide 105 and then a base pair addition at nucleotide 111 which maintained the reading frame of the gene (Table 2).

The mutation to the CipR chromosome of most interest was a frameshift caused by the addition of an "A" at nucleotide 174 to *FTT_0788c*/ *kdsD* (984 bp) (Table 2). KdsD is an arabinose phosphate isomerase, an enzyme that catalyzes the conversion of the pentose pathway intermediate D-ribulose 5-phosphate (R5P) into D-arabinose 5-phosphate (A5P). A5P is a precursor of 3-Deoxy-$_{D}$-*manno*-Octulosonic Acid (KDO), an integral part of the LPS which is an established virulence factor for *F. tularensis* pathogenesis (61-66).

Construction of a *kdsD* mutant in Schu S4. In order to explore the potential role of kdsD in virulence, a *kdsD* mutation in Schu S4 was constructed. We used a modified TargeTron mutagenesis system and the Taergetron plasmid pKEK1140 (Table 1) to disrupt the *kdsD* gene

at site 611|612s using retargeted mobile group II introns as described previously (68). Confirmation of insertion of the intron was demonstrated by PCR analysis using the primers listed in Table 3 that flanked the insert region. For DNA from the Schu S4 strain, a PCR fragment of ~1.3 kb was observed. However for mutant strains that contained the intron insert, a shift of approximately 900 bp was observed (data not shown). To confirm the loss of pKEK1140 from the mutant strain, PCR analysis was performed with primers directed against the plasmid, and no product was observed (data not shown).

As *F. novicida* is frequently used as a surrogate for tularemia studies under BSL-2 conditions, we also examined a mutant for the gene encoding for A5P in the U112 strain from a previously constructed transposon library (69). The homologous gene in the *F. novicida* strain U112 was designated as *kpsF* (*FTN_1222*) (70) which we shall retain for clarity to distinguish between the two *Francisella* species and mutant strains. The *F. novicida kpsF* gene is 969 bp in length and when compared by BLAST (Basic Local Alignment Search Tool) analysis to the *F. tularensis kdsD* gene, the homology between the two genes was 99% identical and 99% positive (data not shown). Two independent transposon mutants were identified having insertions into the *kpsF* gene, one was at position 257 relative to the open reading frame and the other was at position 394 (69). However, we were unable to culture the latter mutant under various growth conditions, therefore all work described here was obtained using the former transposon mutant (BEI catalog # NR-6746).

Minimum inhibitory concentration (MIC) of the *kdsD* mutant and in vitro susceptibility testing. The CipR strain was previously shown to contain alterations in both *parE* and *gyrA* (24) leading to ciprofloxacin resistance (57, 59). To determine if the alteration of *kdsD* in the CipR strain had any role in antibiotic resistance or this mutation occurred spontaneously during the

selection process, MIC values were obtained for the *kdsD* mutant and compared to Schu S4 parent and CipR (Table 4). As expected, no difference in resistance to ciprofloxacin was observed between Schu S4 parent and *kdsD* (MIC = <0.03 ug/ml). High levels of resistance were still detected for the CipR strain (64 µg/ml) as previously reported (24) (Table 4). Likewise, no resistance to ciprofloxacin was observed between the *F. novicida* U112 parent and the *kpsF* mutant (Table 4).

In addition, we examined the *Francisella* mutant strains to determine if inactivation of the *kdsD*/ *kpsF* genes led to increased sensitivity to a panel of hydrophobic agents. As shown in Table 5 for *F. tularensis*, both the CipR and *kdsD* mutant strains showed a significant increase in sensitivity to polymyxin B, Tween 20, and sodium dodecyl sulfate (SDS). Moreover, when the *kdsD* mutant was complemented with a functional gene on a plasmid, the levels of resistance to these compounds were restored to the parent levels. However, no difference in resistance was observed between the parent Schu S4 and both mutant strains in presence of Triton-X 100. The *F. novicida kpsF* mutant was also examined; however, the only inhibitor which the *kpsF* mutant showed an increased sensitivity was Tween 20 (Table 5). This sensitivity could be also restored by complementation.

Exogenous A5P restores growth of the *kdsD* mutant in Chamberlain's defined medium but not CipR. Additional characterization of the strains involved growth analysis in Chamberlain's defined broth medium (CDM). As shown in Fig. 1A, when comparing growth of the CipR and *kdsD* strains to Schu S4, the mutants were able to replicate to some level, but both did show significant differences when compared to the parent for maximum density (p = <0.0001), lag time (p = <0.0001), and maximum growth rate (p = <0.0001), respectively. For the *kdsD* mutant strain, we were able to demonstrate that this growth defect in CDM was due

specifically to the inactivation of the gene. When the *kdsD* mutant strain was complemented with a functional gene in trans on a plasmid, growth levels were completely restored to Schu S4 levels (data not shown). Similar results for growth in CDM with the *F. novicida* U112 parent and *kpsF* mutant strains were observed (Fig. 1B). Overall, the mutant was more impaired for growth and significant differences between the two strains were observed for maximum density (p = <0.0001), lag time (p = <0.0001), and maximum growth rate (p = <0.0001). Complementation with a functional gene was again able to restore growth of the mutant to wild-type levels (data not shown).

As the KdsD/ KpsF enzyme catalyzes the conversion of R5P into A5P, we hypothesized if the growth defects observed in the respective mutant strains of Schu S4 and U112 in Chamberlain's broth could be restored by adding A5P to the media. As shown in Fig. 1 A & B, a significant increase in growth (as measured by maximum density, lag time, and growth rate; p= <0.0001) was observed for both *F. tularensis kdsD* and *F. novicida kpsF* mutants when grown in the presence of 400 μM A5P versus growth without the additional A5P. In contrast, no difference was observed for the respective parent strains when grown with or without additional A5P (Fig. 1A & 1B). Interestingly, the Schu S4 CipR mutant did not show a significant increase in growth with the addition of A5P, despite it also containing a frameshift mutation in *kdsD*. Therefore other mutations are presumably leading to the defect in growth.

The CipR and *kdsD* mutants are affected in O-antigen expression of the LPS and capsule but not lipid A. When performing western blot analysis with lysate material of equivalent bacterial CFU numbers extracted from wild-type Schu S4, CipR or *kdsD* and monoclonal antibodies generated against LPS or the O-antigen capsule, the characteristic profiles of the wild-type strain were not observed in the CipR and *kdsD* mutant strains (Fig. 2A). However, a control

western blot was performed using the same amount of lysate material but probing with an antibody to GroEL, a molecular chaperone, and no difference in no difference in the amount of GroEL was observed between strains. When the *kdsD* mutant strain was complemented in trans with a plasmid containing the functional gene, the LPS and O-antigen capsule profiles were completely restored to this strain (Fig 2A). Similar results were observed by Western analysis with the *kpsF* transposon mutant strain and monoclonal antibody directed against the LPS of *F. novicida* (Fig. 2B). Again, the LPS profile could be completely restored via complementation (Fig. 2B).

Negative ion mode MALDI-TOF mass spectrometry was used to further compare mutant and wild type LPS structures of *F. tularensis*. The MALDI process is capable of fragmenting the glycosidic bond that connects the core oligosaccharide to the lipid A moiety (71), allowing this structure to be elucidated from intact LPS preparations. We observe the prompt fragmentation of LPS and the resultant lipid A species using the data acquisition parameters used in these experiments (Fig. 3). We observe the same lipid A structure and variants as reported by Kanistanon et al (27) where the species at m/z 1665.24 corresponds to the intact lipid A structure shown in Fig. 3. The theoretical m/z for this molecule is 1665.25 [M-H]-. We determined experimental m/z values of 1665.24, 1665.24, 1665.24 and 1665.23 for LPS preparations from cultures of wild type Schu S4, CipR, *kdsD*, and *kdsD* complemented strains, respectively. The species at m/z 1504.2 (delta 161.0 Da) corresponds to the "intact" lipid A structure minus one galactosamine unit. The minor peaks at m/z 1637.2 and 1476.2 correspond to shorter acyl chain lipid A variants (delta 28.0 Da) of the major peaks described above. We observe these same species in all four LPS preparations suggesting that the loss of the KDO structure in the two mutant strains (CipR and *kdsD*) does not impact the structure of lipid A. However, we did

observe a lower intensity of lipid A within the *kdsD* sample which likely resulted from decreased extraction efficiency during sample preparation.

Interaction of *Francisella* strains with macrophage-like cells. The fate of the *F. tularensis* strains following uptake by J774A.1 cells was studied using a gentamicin protection assay. As shown in Fig. 4A & 4B, no difference in the initial recovery of CFUs between Schu S4 and CipR or *kdsD* strains was observed at the 4 hour time point, suggesting the initial uptake of the bacteria was not affected. However, after a 24 hr incubation period, the recovered number of CFUs had increased by several logs for J774A.1 cells infected with Schu S4. In contrast, the number of CFUs recovered from J774A.1 cells infected with CipR (Fig. 4A) or *kdsD* (Fig. 4B) mutant strains had decreased significantly (P=0.0002 and <0.0001, respectively) as compared to CFU counts with the wild-type strain. To demonstrate if this defect in recoverability of the *kdsD* mutant bacteria following macrophage infection was due specifically to the inactivation of this gene, J774A.1 cells were infected with the *kdsD* complemented strain. As shown in Fig. 4B, a several log increase of recovered CFUs from the infected macrophages was observed for the complemented strain.

During these studies, a disruption in the confluence of the macrophage monolayers was noted after the 24 hr incubation with either CipR or *kdsD F. tularensis* mutant strains but not with the parent Schu S4 or *kdsD* complemented strains (Fig. 4C). Previous studies with other *F. tularensis* mutants containing LPS defects had shown similar induction of macrophage death (72, 73). Therefore, the loss of CFU recovery with the *F. tularensis* mutants from our current study could be due to a loss of the ability to grow intracellularly or by loss of the host and intracellular replicative niche.

Similar results were observed when examining the recovery of CFUs with the *F. novicida* *kpsF* mutant from infected J774A.1 cells. As shown in Fig. 5A, a several log CFU increase was observed with the U112 wild-type strain 24 hours-post challenge. In contrast, no increase in the CFUs was observed with the *kpsF* mutant and thus differed significantly different from the wild-type strain (P=0.0042). However, when a functional gene was supplied to the mutant via complementation, CFU recovery was restored to the mutant strain. The fate of the macrophages infected with the *F. novicida* LPS mutant was also examined. However, we demonstrated that cell death was occurring via apoptosis as detected by caspase-3/7 activity (Fig. 5A & 5B). The J774A.1 cells infected with the *kpsF* mutant strain were found to be undergoing apoptosis at a much higher level than observed with cells infected with the U112 strain or uninfected macrophages. However, if the mutant was complemented, little apoptosis was observed (Fig. 5A & 5B).

The CipR and *kdsD* mutants of *F. tularensis* were highly attenuated in mice. To determine if the CipR and *kdsD* mutant strains were still virulent in mice, various models of tularemia challenges were tested: intradermal, intranasal, and small particle aerosol exposure. The murine LD_{50} measurements for the wild-type strain by intranasal and intradermal challenges were both determined to be 1-2 CFU (Fig. 6 A & 6B; Table 6). In contrast, the LD_{50} values for the CipR mutant by these same challenge routes were greatly increased: 14,000 and >49,000 CFU, respectively (Fig. 6C & 6D; Table 6).

Likewise, complete attenuation was observed for mice challenged by the intranasal and intradermal routes for all challenge doses with the *kdsD* mutant. LD_{50} measurements for the *kdsD* mutant were >36,000 and >82,000 CFU, respectively (Fig. 6 E & 6F; Table 6). To demonstrate this severe attenuation was due specifically to the inactivation of the *kdsD* gene,

mice were intranasally challenged with the complemented mutant (Fig. 6G; Table 6). Almost complete restoration of virulence was observed when mice were challenged by the intranasal route with a complemented *kdsD* strain, with the LD_{50} determined to be <10 CFU (Table 6).

The recovery and dissemination of the CipR and *kdsD* mutants were hindered after intranasal challenge. To determine the fate of the CipR and *kdsD F. tularensis* mutants after challenge intranasally, groups of mice were separately exposed to wild-type Schu S4 (131 CFU), CipR (1,750 CFU), or *kdsD* (6,000 CFU). At set time points after challenge, mice from each group were euthanized for determining either bacterial burden from lungs and spleens (Fig. 7) or assessing histopathological changes (Fig. 8).

For mice receiving the wild-type Schu S4, the number of bacteria recovered from the lungs and spleens increased exponentially after Day 1. On Day 3, approximately 10^7 CFU/ g were recovered for both the lungs and spleens. By Day 5, all mice were moribund and one had succumbed to infection. For the remaining mice, lungs and spleens contained approximately 10^9 CFU/ g in the lungs and spleens (Fig. 7). In contrast, the recovery of CFUs from organs and the ability of CipR and the *kdsD* mutant strains to disseminate from the lungs were severely affected as compared to mice challenged with the Schu S4 parent strain. For the lungs over the first 7 days of testing, little change in the recovered CFUs was observed as compared to CFUs at 6 hours post-challenge. At the end of the study on Day 28, the remaining challenged mice were tested for the presence of bacteria within their organs. On Day 26, two of the CipR challenged mice had succumbed to infection. The lungs from the remaining CipR challenged mice were still shown to contain some CFUs but still at a relatively low level. All of the *kdsD* challenged mice survived until Day 28, and the lungs of these mice were found to be free of *F. tularensis* (Fig. 7).

As shown in Fig. 7, overall very few of the spleens of the CipR or *kdsD* mutant challenged mice had any CFUs recovered over the first 2 days. Over the remaining week of testing, the number of spleens still shown to contain any CFUs was inconsistent, with many being sterile for the presence of *F. tularensis*. At the end of the study, one of the spleens from the CipR challenged mice had low levels of CFUs recovered. However, none of the spleens for the *kdsD* challenged mice had bacteria present.

Along with testing for the presence and trafficking of *F. tularensis* from the lungs, additional mice were processed to compare histopathological differences in disease progression following intranasal challenge with the wild type Schu S4 or the two mutant strains (Fig. 8). All pathology images in Fig. 8 are for Day 5 post-challenge. It is at this time point that all wild-type challenged mice become moribund versus complete survival for the mice challenged with the CipR or *kdsD* mutant strains.

When examining organs from mice on day 1 post-challenge with Schu S4, the mice did not have any lesions suggestive of tularemia. The lesions in these animals were limited to non-specific hyperplasia of lymphoid tissue in various lymph nodes and in the white pulp of the spleen. However, by day 3 post-exposure, mice demonstrated classic lesions consistent with peracute infection for tularemia (19, 21, 74). These lesions consisted of small multifocal random areas of neutrophilic inflammation in the sinusoids of the liver, red and white pulp of the spleen, cortex and medulla of the lymph nodes, and interstitium of the lung. These neutrophilic infiltrates were often associated with areas of tissue necrosis. These random areas of neutrophilic inflammation are consistent with embolic (vascular) spread of *F. tularensis*. It is likely that these lesions represent an early time point in the pathogenesis of *F. tularensis*, prior to widespread colonization of tissues and associated tissue necrosis. For mice on day 5 post-exposure, classic lesions consistent with acute to subacute infection with *F. tularensis* were observed (Fig. 8). These lesions consisted of random foci of lytic necrosis in the liver, spleen, lungs, and lymph nodes with

neutrophilic inflammation (Fig 8). Additionally, these necrotic areas are associated with numerous large colonies of coccobacilli, morphology consistent with *F. tularensis.*

When examining mice receiving the CipR strain, no lesions were observed indicative of *F. tularensis* infection on day 1. However by Day 2 post-exposure, 2/3 mice have minimal multifocal neutrophilic inflammation with necrosis in the lung (pneumonia), typical of tularemia. This lesion is characterized by effacement of lung parenchyma and replacement by necrotic debris and neutrophilic inflammation. The areas of necrosis and inflammation in the lung appeared to be random and associated with small airways (alveoli) around bronchioles and vessels. Similar *F. tularensis* induced pneumonia is noted in all day 3 mice. In all Day 4 mice, there is similar minimal to mild *F. tularensis* induced pneumonia with extension to the surface of the lungs (pleura), and admixed with the necrosis and neutrophils are discernible histiocytes/macrophages. Additionally, in 2/3 Day 4 post-exposure mice, there is minimal multifocal hepatocyte degeneration and necrosis with some neutrophilic inflammation. In all Day 5 post-exposure mice, there was mild to moderate *F. tularensis* induced pneumonia with extension to the surface of the lungs (pleura) and admixed with the necrosis and neutrophils are discernible histiocytes/macrophages (Fig. 8). The pneumonia in the Day 5 mice progressed to being more severe as 10-25% of the lung parenchyma tissue was affected versus less than 10% which was observed for Day 2 through Day 4 mice. In 1/3 mice from the Day 5 post-challenge, there was minimal focal necrosis with neutrophilic inflammation in the liver (Fig. 8). In all three Day 6 post-exposure mice, there was similar mild to moderate neutrophilic and necrotic pleuropneumonia (pneumonia that extends to the surface (pleura) of the lung) with admixed histiocytic (macrophages) and lymphoplasmacytic inflammation. In 2/3 mice from Day 6 post-exposure mice, there was minimal multifocal hepatocyte degeneration and necrosis with some neutrophilic inflammation. At the end of study at Day 28, there were diffuse mild to moderate to marked lymphoplasmacytic and histiocytic pleuropneumonia with some neutrophils associated with the aforementioned inflammatory infiltrate in the lung parenchyma and within bronchiolar lumina. This inflammation was more chronic with a minimal active component, which indicates the lung inflammation may be resolving. There was minimal lymphoid hyperplasia in the white pulp of the spleen

in all mice, which may be due to chronic antigenic stimulation from resolving *F. tularensis* infection. Similar lymphoid hyperplasia was observed in 2/5 Day 28 mice in the tracheobronchial lymph node, likely due to chronic antigenic stimulation from *F. tularensis* infection of the lungs. In 4/5 mice, there was minimal multifocal lymphoplasmacytic, histiocytic, and neutrophilic inflammation in the liver. Similar to the inflammation in the lung, this inflammatory response was more chronic in nature with a minimal active component, suggesting the liver inflammation may be resolving. It should be noted that all of the *F. tularensis* challenged mice were compared to mice receiving only PBS intranasally for comparison, and no lesions were noted in any of the organs (data not shown).

Overall a similar pattern of disease was observed for mice challenged intranasally with the *kdsD* mutant as described above for the CipR mutant. Mice that were sacrificed on Day 1 again demonstrated effacement of lung parenchyma and replacement by necrotic debris and neutrophilic inflammation. The areas of necrosis and inflammation in the lung appear to be random and associated with small airways (alveoli) around bronchioles and vessels. In all mice in this group, the severity was judged to be only minimal. In addition, all three mice had lymphoid hyperplasia of the submandibular lymph node and 1/3 had hyperplasia of the white pulp (lymphoid tissue) of the spleen. Day 2 mice had similar lung lesions that were of minimal severity in all cases. There was lymphoid hyperplasia of the submandibular lymph node in all three mice and lymphoid hyperplasia of the spleen and mesenteric lymph node in 1/3 mice. By Day 3 post-infection, the pneumonia was slightly more severe, scoring mild in two mice and moderate in one mouse. The infection in the Day 3 mice extended to the pleural surface in 2/3 mice and affected pulmonary vessels in all three. The character of the lesion was still primarily necrosis with infiltration by neutrophils, but in two mice, histiocytes/macrophages were also observed. Lymphoid hyperplasia of the mesenteric lymph node was observed in only one mouse in this group. Within the Day 4 group, the pneumonia also involved the pleural surface in all

three mice, and the pneumonia ranged from minimal to moderate in severity. The character of the inflammation was still mainly necrosis with neutrophils and macrophages, but this was the first time point where lymphocytes and plasma cells were observed, indicative of more chronic immune response. Additionally on Day 4, the bacterial infection had seeded to the liver resulting in random areas of infiltration by neutrophils and macrophages with variable degeneration and necrosis of hepatocytes. Lymphoid hyperplasia of the submandibular lymph node was observed in a single mouse. In the Day 5 samples, mild pneumonia was present in all mice, but unlike the previous groups there was no evidence of necrosis (Fig. 8). The inflammation was primarily neutrophilic and histiocytic but with a prominent lymphoplasmacytic component that often formed cuffs around blood vessels in the lungs, indicative of a resolving pneumonia. In addition, all mice in this group had a mild hepatitis similar to that seen in the Day 4 group (Fig. 8). Lymphoid hyperplasia was slightly more common in this group, occurring in 2/3 mesenteric lymph nodes and 1/1 submandibular lymph nodes. For Day 6 mice, pneumonia and hepatitis were present in all mice. Like the Day 5 group, there was no longer necrosis in the lung, but more chronic inflammation (lymphocytes and plasma cells), suggestive of a resolving process. The severity of the pneumonia was mild in two mice and mild to moderate in the third. The hepatitis was also more lymphocytic in character, indicative of resolution (Fig. 8). Lymphoid hyperplasia was only observed in the mesenteric lymph node of a single mouse. At the end of the experiment on Day 28, 2/3 mice still had evidence of inflammation in the lungs. The inflammation was mostly lymphoplasmacytic and histiocytic and was located around vessels, bronchioles and within the pleura, and the severity ranged from minimal to mild. No necrosis was evident.

The CipR and *kdsD F. tularensis* mutants are attenuated by aerosol challenge for mice. As aerosol exposure of *F. tularensis* is the greatest threat from a biodefense perspective, the ability of the CipR and *kdsD* mutant strains to be aerosolized and cause infection in mice was also explored. Since both mutant strains were highly attenuated via the intranasal route of challenge, mice were exposed to a single high dose of *F. tularensis* via small particle aerosol. All mice survived exposure to the CipR (the equivalent of 43 wild-type LD_{50}) or *kdsD* (the equivalent of 100 wild-type LD_{50}) mutant strains for 21 days (Fig. 9). In contrast, all mice receiving aerosolized Schu S4 (33 LD_{50}) succumbed to infection by Day 5 (Fig. 9). The LD_{50} for BALB/c by aerosol challenge with the Schu S4 strain is approximately 300 CFU (19, 20).

To determine what, if any, pathological changes occurred in mice surviving aerosol challenge with the mutant strains as compared to mice exposed to the wild-type Schu S4 strain, mice were euthanized when moribund by Day 5 or following survival 21 days post challenge (CipR and *kdsD* mutant challenged mice) and processed for histopathologic examination. For mice challenged with the wild-type Schu S4 strain, the microscopic lesions were typical of *F. tularensis* and resulted in the death of these mice. The most significant lesions were noted in the spleen and the lung. The lesion in the spleens is characterized by necrosis in the red and white pulp of the spleen with associated acute neutrophilic inflammation and fibrin (Fig. 10). In the lung, the lesion is characterized by necrosis and neutrophilic inflammation (necrosuppurative) of the parenchyma and pleura (surface of the lung). There is also mild to moderate inflammation of lung vessels (vasculitis) characterized by necrosis and neutrophilic inflammation within vessel walls, often with fibrin thrombi (Fig. 10). Examinations of the liver of the moribund mice consisted of multifocal, minimal to mild necrosis with associated neutrophilic inflammation and intracellular coccobacilli (Fig. 10). Other lesions in the mice were typical of tularemia to include

bone marrow necrosis, nasal turbinate/pharyngeal mucosal necrosis, lymph node necrosis, and/or fibrin thrombi in various organs (data not shown).

For mice challenged by aerosol with the CipR mutant, the only microscopic lesion of note in all mice examined was a lymphoplasmacytic and histiocytic pleuropneumonia with some neutrophils associated with the inflammatory infiltrate in the lung parenchyma and within bronchioles (Fig. 10). This inflammation is more chronic with a minimal active component and suggests the lung inflammation may be resolving following *F. tularensis* infection. There is minimal lymphoid hyperplasia in the white pulp of the spleen which may be due to chronic antigenic stimulation from resolving *F. tularensis* infection (Fig. 10). Likewise for mice surviving aerosol challenge with the *kdsD* mutant, a very similar course of disease for the mice was observed as described above for the CipR strain. The one slight difference was that the inflammation in the lungs of the mice sprayed with the CipR strain may be slightly more severe based upon subjective assessment of the amount of lung parenchyma affected. Overall for the lungs of the *kdsD* sprayed mice, there was minimal to mild lymphoplasmacytic and histiocytic inflammation with few scattered neutrophils, often associated with bronchioles in the lung (Fig. 10). The inflammation is indicative of a chronic resolving process from aerosol exposure to the *kdsD* mutant. Finally, no other lesions or pathologic changes were noted in the liver or spleens of the mice surviving aerosol challenge with CipR or *kdsD* mutant in contrast to the severe pathologic changes observed with mice succumbing to infection with the wild-type Schu S4 strain (Fig. 10).

The *kpsF* mutant of *F. novicida* is highly attenuated for mice. As *F. novicida* is frequently used as a surrogate for tularemia studies, we wished to demonstrate if the *F. novicida* *kpsF* mutant was also attenuated in a murine model of inhalational tularemia to further

463 corroborate the studies performed with the *kdsD* mutant in *F. tularensis* described above. As
464 shown in Fig. 11 and Table 6, we challenged groups of mice intranasally with either the *F.*
465 *novicida* U112 parent strain or the *kpsF* transposon mutant. All mice receiving the parent strain
466 succumbed to infection, and the LD_{50} was >24 CFU (Fig. 11 & Table 6). However, mice
467 receiving the *kpsF* mutant were able to survive challenge except for those receiving the highest
468 mutant doses (Fig. 11). The LD_{50} for the *kpsF* mutant was calculated to be 25,119 CFU (Table
469 6). The attenuation observed for the *kpsF* mutant was able to be almost fully restored when a
470 functional gene was supplied in trans on a plasmid (Fig. 11). The LD_{50} for the complemented
471 strain was calculated to be 32 CFU (Table 6).
472
473 **Discussion:**
474 Bacterial resistance to antibiotics is a serious threat to both public health and biodefense
475 communities. The purpose of this study was to further characterize a ciprofloxacin resistant
476 mutant of the Schu S4 strain of *F. tularensis* (24) to better understand the pathogenesis and
477 potential threat posed if such a strain emerged, naturally or intentionally. The major findings of
478 our work were: 1) The CipR mutant was severely hampered in its ability to cause infection in all
479 tested murine models of tularemia; 2) In addition to the previously identified changes to *gyrA*
480 and *parE* (24), the genome of the CipR strain contained additional alterations. The mutation
481 most likely leading to the attenuation to the CipR mutant was a frameshift in *kdsD*, a
482 biosynthesis gene for KDO; 3) Mutation of *kdsD*/*kpsF* in the Schu S4 strain of *F. tularensis* or
483 the U112 strain of *F. novicida* led to LPS alterations and severe attenuation in mice for both
484 *Francisella* species.

In addition to having a high level of resistance to ciprofloxacin, the CipR strain displayed numerous other phenotypes: in vitro growth defects broth media, increased sensitivity to a panel of hydrophobic agents, alteration of the LPS profile, premature induction of macrophage death, and high attenuation in multiple models of murine tularemia. Many of these additional phenotypes (but not all) are likely due to the frameshift of *kdsD* gene which occurred coincidently during the selection process and was unassociated with ciprofloxacin resistance. Mutations specifically to the *kdsD*/ *kpsF* gene of either the parent Schu S4 strain of *F. tularensis* or the U112 strain of *F. novicida* replicated many of the observations observed with the CipR strain. We focused on the mutation of *kdsD* in CipR to better understand the phenotype of this strain since it was the only gene, outside of *parE,* experiencing a frameshift which presumably would result in a higher impact effect. In addition, LPS is an established virulence factor for *F. tularensis* (61-66).

The other altered genes on the CipR chromosome led to amino acid substitutions within the effected protein (Table 2) versus undergoing a more dramatic frameshift mutation. This would not discount the potential of these other mutations playing some part in the loss of virulence or other phenotypes observed for the CipR strain. Some of these alterations occurred to genes encoding for other known *Francisella* virulence factors, such as *Ftt_0807*/ *capA* (75, 76) and *fupA* (77, 78). In addition, the role, if any, in *Francisella* pathogenesis for the other proteins remains to be determined. The FabH and FabF proteins are both enzymes involved in type II fatty acid biosynthesis system which are required for synthesis of essential lipoproteins, phospholipids, and LPS (79, 80). Presently, little else is known about FtaG (FTT_1573c), an outer membrane surface antigen (81). Likewise, *Ftt0_676* encodes for an ion transporter which has been shown to be downregulated when *F. tularensis* is present within macrophages (82).

In addition, as shown in Fig. 1A, the broth growth defects of the *kdsD* mutant in Schu S4 and *kpsF* mutant in U112 were able to be restored to the respective wild-type levels when providing exogenous A5P, the end product of the $_{D}$- arabinose 5-phosphate isomerase activity. This growth defect was not able to be restored to the CipR strain when providing A5P, demonstrating additional defects to this strain.

However, many of the observations for CipR were also seen in the Schu S4 *kdsD* mutant, such as a defect in the LPS profile. This would not be surprising as the *kdsD* gene encodes for the first step for biosynthesis of KDO. Our study is the first to examine a *kdsD* mutant of *F. tularensis*. However, a recent report describes a transposon mutant in *kdsB* (*FTT_1478c*) which encodes for cytidine 5'-monophospho-KDO synthase. This mutant also did not react with antibodies generated against LPS or the capsule but virulence studies were not reported (72). Other studies describe additional LPS *Francisella* mutants in LPS biosynthesis, and these mutations also show early induction of death to macrophages (72, 73) and attenuation in murine models of tularemia (64, 83, 84), as observed for the CipR mutant and the *kdsD* mutant reported here.

In our current study, the pathology noted with mice challenged intranasally or by small particle aerosol with the wild-type Schu S4 are in general agreement with other published studies (19, 74). For pneumonic tularemia by either challenge route with Schu S4, overall, the lungs of infected mice showed lesions characterized by necrosis and nueurtophilic inflammation of the parenchyma and pleura. The lesions in the spleens were characterized also by necrosis of the red and while pulp. The BALB/c mice were extremely sensitive to challenge by the intranasal route with Schu S4 as the LD_{50} was determined to be only 1-2 CFUs. In contrast, mice that were intransally challenged with the CipR strain or the *kdsD* mutant were highly resistant (Table 6).

However, when the intranasal challenge doses for the CipR mutant reached the range of ~10,000 CFUs, 3/10 mice did succumb by Day 16, a much later time point than observed with wild-type Schu S4 challenged mice succumbing to infection by Day 5 when exposed to the highest challenged dose (300 CFU). However, no mice challenged with the *kdsD* mutant succumbed to infection or showed any outward clinical signs, even at the highest challenge dose (82,000 CFU). Therefore, though both the CipR and *kdsD* mutant strains are highly attenuated as compared to the Schu S4 parent strain, the *kdsD* mutant does appear to be slightly more affected for virulence for pneumonic challenge models. This was also reflected in the pathology results for the aerosol challenged mice where a slight in increased lung inflammation was noted in the lungs of the CipR challenged mice as compared to the *kdsD* challenged mice. In addition, the mice challenged with the *kdsD* mutant were estimated to have received over twice the dose as compared to the CipR challenged mice. The exact reasoning for this slight difference in the level of attenuation between CipR and *kdsD* remains to be determined and was unexpected as the CipR strain contains additional genetic changes. Potential reasons for this difference could be that the CipR challenged mice are able to mount more of an immune response to the mutant strain since these bacteria from the lungs could be recovered for a longer period of time (Fig. 7).

Other LPS (*waaY* and *waaL*) mutants in a Schu 4S background similarly showed high levels of attenuation in BALB/c mice following intranasal challenge as determined by LD_{50} measurements ($1.3x10^4$ and $3x10^3$, respectively) (64). However, we note several differences in the infection of BALB/c mice between the mutant strains. The Schu S4 *waaY* and *waaL* mutant strains examined in by Rasmussen et al (64) appears to have induced a much higher level of lung necrosis as examined by histopathological analysis when challenged with 10^6 CFU of either mutant strain. In contrast, the *kdsD* mutant showed only a low level of pneumonia early on

following intranasal challenge which was much less severe when compared to infection with the parent Schu4 strain. However, our challenge dose was with the *kdsD* mutant was $6x10^3$ CFU.

In addition, the *waaY* and *waaL* Schu S4 mutants were able to disseminate from the lungs and replicate within the mouse organs examined (64). For out study, the *kdsD* mutant was recovered poorly from the spleens following intranasal challenge and in addition, CFUs recovered from the lung did not increase over the time course examined.

Two possibilities exist to explain these differences between the two studies. Firstly, the *waaY* and *waaL F. tularensis* mutants expressed a truncated LPS structures and retained a partial O-antigen structure (64). In contrast, the *kdsD* mutant is unable to synthesize KDO; therefore no O-antigen structure would be expressed at all (Fig. 2). The *kdsD* mutant with a more dramatic LPS deficiency could be more attenuated for the murine challenges. Secondly, the doses used for the mouse challenges with the mutant strains between the two studies differed (10^6 CFUs for *waaY* and *waaL* versus 10^3 CFUs for *kdsD*) making a direct comparison difficult.

Other LPS mutants of *F. tularensis* demonstrated the potential to provide a protective response against parent strain challenges (64, 66, 83, 85-87). Future vaccination studies with the Schu S4 *kdsD* mutant may be warranted to determine if some level of protection would be provided against challenge with fully virulent *F. tularensis* strain. Although, as detailed above, the dissemination and recovery of the *kdsD* mutant was rather limited (Fig. 7) as compared to the dissemination of other Schu S4 LPS mutant strains which were able to protect (64). Therefore protection granted with the *kdsD* mutant as a live vaccine could be limited.

However, a more promising avenue to explore further is the potential of $_D$- arabinose 5-phosphate isomerase (KdsD) to serve as a therapeutic target as previous proposed (88, 89). This enzyme would be an attractive target for novel therapeutics for gram-negative bacteria as KDO is

necessary for LPS synthesis and bacterial virulence. In addition, arabinose-5-phoshate would not be present within mammalian tissue to provide an exogenous source. Furthermore, structural analyses studies have identified putative active sites for catalysis (90, 91), opening the possibility for the screening of small molecule inhibitors for drug design. Such novel targets and mechanisms of action are currently needed to combat antimicrobial resistance.

Materials and Methods:

Bacterial strains. All strains and plasmids used in this study are listed in Table 1. *Escherichia coli* NEB Turbo cells (New England Biolabs) were used for cloning purposes. *E. coli* was propagated in Luria broth or agar supplemented with ampicillin at 100 μg/ml, hygromycin at 200 μg/ml, or kanamycin at 20 μg/ml as necessary. All cultures were grown at 37°C.

The *F. tularensis* subsp.*tularensis* strains used included the fully virulent Schu S4 (21) and a ciprofloxacin resistant Schu S4 derivative which has been previously selected with approval by the CDC (24). Previous characterization of the ciprofloxacin resistant strain determined that the *gyrA* gene contained two base pair (bp) switches: C248→T and G259→T. In addition, a five-bp deletion occurred in the *parE* gene. Also included was *F. tularensis* subsp. *novicida* strain U112 and a transposon derivate (69) (BEI).

For routine growth of *F. tularensis* species, bacteria were grown on enriched chocolate agar plates obtained from Remel™ (product number R01300; Lenexa, KS). When necessary, agar was supplemented with kanamycin at 10 μg/ml and/ or hygromycin at 200 μg/ml. As indicated, *F. tularensis* was grown in broth culture in Chamberlains Defined Medium (CDM)

(92) or brain heart infusion (BHI) broth supplemented with 1% Isovitalex (Becton Dickinson, Cockeysville, MD, USA).

USAMRIID is compliant with all federal and Department of Defense regulations pertaining to the use of Select Agents.

Genomic sequencing and analysis. Chromosomal DNA was prepared from the ciprofloxacin resistant *F. tularensis* using the Qiagen Genomic-tip 500/G kit with the appropriate buffers according to the manufacturer's instructions. Genomic DNA (gDNA) was sequenced at on a Pacific Biosciences RSII. Specifically, the sequencing library was prepared using the SMRTbell™ Template Prep Kit (Pacific Biosciences, Menlo Park, CA) following manufacturer's protocol. 5 μg of gDNA was fragmented using gTUBE (Covaris Inc., Woburn, MA) to ~20 kb. After DNA damage repair and ends repair, blunt hairpin adapters were ligated to the template, and failed ligation products were digested with ExoIII and ExoVII exonucleases. Resulting SMRTbell template was size selected on BluePippin system (Sage Science, Beverly, MA) using 0.75% dye-free agarose cassette with 4-10kb Hi-Pass protocol and low cut set on 4 kb. Size selected template was cleaned and concentrated with AMPure PB beads. The P4 polymerase in combination with the C2 sequencing kit and we collected 240-minute movies. Raw reads were quality filtered (subread length >= 500; polymerase read quality >= 0.80) and assembled using HGAP 2 v2.1.0 with a length cutoff of 14,211 bp (93). Gepard v1.30 (94) was used to identify repetitive, low-quality sequence at the contig ends, which was trimmed using custom scripts. The final genome assembly (Genbank: CP013853) was annotated using NCBI's Prokaryotic Genome Annotation Pipeline v3.0 (95).

To identify genomic differences in *F. tularensis* CipR relative to its parent strain, wgsim (github.com/lh3/wgsim) was used to computationally "shred" the *de novo* assembly into 1

622 million perfect-match read pairs (150bp x 2 with a fragment size of 500bp), for an average of
623 ~150x depth. These synthetic reads were then aligned to the *F. tularensis* Schu S4 reference
624 genome (Genbank: NC_006570) using Bowtie2 (reads were ignored if they mapped equally well
625 to multiple places in the reference genome) (96) and variants were called using the
626 UnifiedGenotyper in GATK v3.1-1-g07a4bf8 (97). The predicted effects of variants were
627 annotated with SnpEff (98) using the " Francisella_tularensis_SCHU_S4_uid57589" database.

628 Mutant Construction. The *kdsD* mutant strains of *F. tularensis* were created using a
629 modified TargeTron (Sigma-Aldrich, St. Louis, MO) mutagenesis system (68). In brief, the
630 coding sequence of the gene of interest was entered into the Sigma TargeTron primer design site
631 to determine the appropriate oligonucleotides for retargeting the intron. The modification to this
632 procedure was an *Xho*I restriction site was substituted for the *Hind*III. The resulting PCR
633 product was cloned into vector pKEK1140 (68). The plasmid was introduced into the Schu S4
634 strain by electroporation and the transformed strains with the retargeted plasmid were grown at
635 30°C on chocolate agar with 15 µg/ml kanamycin. Kanamycin resistant colonies were then
636 isolated and screened via PCR to identify mutant strains. The presence of the TargeTron
637 insertion was determined using an intron-specific EBS universal primer combined with a gene
638 specific primer, and intron insertion of the targeted gene was determined using gene-specific
639 primers that amplified across the insertion site. To cure the plasmid from the mutant clones,
640 bacteria were grown overnight at 39^{o}C in BHI containing 1% Isovitalex and serially diluted on
641 chocolate agar plates. Individual colonies were screened for loss of kanamycin resistance.

642 Complementation of the *kdsD* mutation. For complementing the observed phenotypes
643 from the *kdsD F. tularensis* and *kpsF F. novicida* mutant strains, a functional *kdsD* gene was
644 PCR amplified from DNA from the Schu S4 strain with flanking upstream DNA which would

presumably contain the promoter. The DNA fragment was cloned into vector pMP831 (99) and then transformed into the respective mutant strains by electroporation. The constructs were selected by hygromycin resistance (200 µg/ml) which is present on the vector.

Growth assays. Growth assays were performed in Chamberlains defined broth (92), with or without the addition of D-arabinose 5-phosphate (A5P) (Sigma-Aldrich, product # A2013), as indicated. Assays were performed using an Infinite M200 Pro (Tecan; Männedorf, Switzerland) microplate reader in 96-well microtiter plates at 37^{o}C with shaking. The OD_{600} was measured every 60 min. For all assays, the bacterial strains were grown for 24 hr on a chocolate agar plate and then resuspended in the respective broth medium to an equal OD_{600}. All samples were performed in quadruplicate and included medium controls to confirm sterility and for use as blanks to calculate the absorbance of the cultures.

Macrophage Assays. J774A.1 cells, a murine macrophage-like cell line, were seeded (~2.5x10^{5} cells/well) into 24-well plates and cultured 2-3 days (37°C, 5% CO_2) at which time the cells had formed confluent monolayers. The cells were maintained in Dulbecco's Modified Eagle's medium (D-MEM) containing high glucose, 10% heat-inactivated fetal bovine serum (FBS), plus 1.5 g/l sodium bicarbonate. For the intracellular assays, *F. tularensis* or *F. novicida* was suspended in PBS from a 24 hr or 18 hr plate, respectively, and then diluted 1:5 in tissue culture medium. The bacterial suspension was added to the macrophages in 200 µl to achieve an MOI of ~100:1. The bacteria and macrophages were allowed to coincubate for 2 hrs at 37^{o}C with 5% CO_2. Next, the medium containing the extracellular bacteria was aspirated and replaced with fresh tissue culture medium supplemented with 25 µg/ ml of gentamicin for an additional 2 hrs. After this incubation, a sample of tissue culture wells was washed three times with PBS. The monolayer was then lysed with 200 µl of sterile water, immediately scraped, and suspended

668 in 800 µl of PBS. The suspension was serially diluted in PBS and plated onto Remel™
669 chocolate agar plates.

670 To analyze the fate of the macrophages infected with Schu S4 strains, coverslips
671 containing the J774 cells were fixed with 4% formalin, permeabilized with PBS containing
672 0.025% saponin and then subjected to Wright Giemsa solution (Electron Microscopy Sciences,
673 Hatfield, PA) for 10 min. Coverslips were washed 3x with PBS and mounted. Light microscopy
674 was performed on the Zeiss Axio Observer Z1 equipped with a x 40 oil objective lens, AxioCam
675 HRc camera and Zen-Blue edition 2011 software (Carl Zeiss Microimaging, Thornwood, NY).

676 For analysis of macrophages infected with *F. novicida*, coverslips were removed and
677 placed in media containing 1 drop of Cell Event Caspase 3/7 green ready probes reagent
678 (Thermo Scientific Fisher) and incubated for 30 minutes. Confocal microscopy was performed
679 on the Zeiss 700 Laser Scanning Microscopy System using Zen-Black Edition 2011 software
680 (Carl Zeiss Microimaging, Thornwood, NY). Fluorescent and differential interference contrast
681 (DIC) images were collected using the ×40 (numerical aperture: 1.3) oil objective lens with the
682 pinhole set to 2 Airy unit.

683 Analysis of bacterial cell extracts. Whole-cell extracts were collected for protein and
684 endotoxin analysis from plate grown *F. tularensis* and *F. novicida* strains. Cultures were
685 prepared at equal CFU concentrations in PBS, lysed in gel loading buffer solution, and boiled for
686 30 min. Sterility of the extracts was confirmed. Proteins were fractioned on NuPage Novex 4-
687 12% Bis-Tris gels. For Western analysis, fractionated proteins were transferred onto a
688 nitrocellulouse membrane using an iBlot Gel Transfer Device. After transfer, the membranes
689 were blocked with 1% skim milk in Tris Buffered Saline + Tween 20. *F. tularensis* samples
690 were blotted with mouse monoclonal antibodies, anti-LPS (F6070-02X; US Biological) or anti-

capsule (11B7; (61)), at a dilution of 1:500. *F. novicida* samples were blotted with a mouse monoclonal antibody from cell culture supernatants with an anti-LPS antibody, Fn#13, (ImmunoPrecise Antibodies) at a dilution of 1:100. The loading control antibody used for all analyses was rabbit polyclonal anti-*E.coli* GroEL (dilution of 1:2,000) (Enzo Life Sciences). Bands were visualized using 3,3',5,5'-Tetramethylbenzidine (TMB) Membrane Peroxidase substrate (Kirkegaard & Perry Laboratories, Inc; Gaithersburg, MD).

Mass spectrometry analysis of lipid A. LPS from *F. tularensis* strains was prepared using a LPS extraction kit (Catalog # 17141) from Intron Biotechnology. Sterility of the LPS preparations was confirmed. The samples were analyzed by matrix-assisted laser desportion ionization time-of-flight (MALDI-TOF) mass spectrometry analysis using protocols developed by Zhou et al (100). In short, 20 µl of each LPS sample was mixed with 80 µl of methanol/chloroform in a glass vial, briefly vortexed and 1 µl of the solubilized sample spotted on a stainless steel target. Samples were allowed to air dry and 0.5 µl of matrix (10 mg/ml 2,5-dihydrobenzoic acid) was added to each spot. Samples were analyzed by MALDI-TOF mass spectrometry in reflector/negative ion mode using an Applied Biosystems 5800 instrument. The instrument was calibrated with low molecular weight standards (Bruker) and data were collected from 800 to 4000 (m/z) by manual “hot spot” searching and adjusting laser intensity to obtain optimum signal to noise for each sample. Each of the reported spectra are averages of 1000 laser shots.

MIC susceptibility assays. Ciprofloxacin was purchased from USP, made into 5mg/mL stocks according to the CLSI guidelines (Clinical and Laboratory Standards Institute, 2013), and stored at -70^{o}C until use. Bacterial inoculums were prepared by suspending colonies into cation-adjusted Mueller-Hinton broth (CAMHB) from isolates grown aerobically at 35^{o}C on chocolate

agar plates for 42-48 h. Suspended cultures were diluted with CAMHB to a bacterial cell density of ~10^6 CFU/ml based using a 0.5 McFarland standard. To each well of the 96-well plate, 50 µl of the adjusted dilution was added for a final inoculum of approximately 5 x 10^4 CFU/well. MICs were determined by the broth micro-dilution method in 96-well plates according to CLSI guidelines (Clinical and Laboratory Standards Institute, 2013). Ciprofloxacin serially diluted two-fold in 50 µl of CAMHB. The antibiotic range tested was 0.03 – 64 µg/ml based on a final well volume of 100 µl after inoculation. Plates were incubated at 35^{o}C and MICs determined visually at 42- 48 h. Quality control was established by using *E. coli* ATCC 25922, *S. aureus* ATCC 29213, and *P. aeruginosa* ATCC 27853 according to CLSI guidelines (Clinical and Laboratory Standards Institute, 2013).

in vitro susceptibility assays *F. tularensis* and *F. novicida* strains were suspended in PBS at an OD_{600} of approximately 0.2 and 100 µl aliquots were spread on chocolate agar plates. Sterile paper disks (Sigma, product # 74146) 10 mm in diameter were saturated in water, SDS (100 mg/ ml), Triton X (5%), Tween 20 (5%), or PMB (10 mg/ ml), allowed to dry, and placed onto chocolate agar plates. For each study, three separate disks were prepared for each inhibitor was assessed by measuring the diameter of the zone of growth inhibition. The study was repeated three separate times.

Animal challenges. To determine the ability to cause infection, BALB/c mice (7-9 week-old) were challenged with *F. tularensis* or *F. novicida* in groups of 10 by various routes. For all methods of infection, the challenge doses were determined by serial dilutions in PBS and plating on chocolate agar. Intradermal challenge. Frozen *F. tularensis* stocks were streaked onto chocolate agar and incubated at 37^{o}C for 2 days. Next, a fresh chocolate agar plate was swabbed from the streak plate and grown for 24 hr. Bacterial cells were harvested from the plate in PBS,

and mice were challenged with 0.1 ml aliquots at various cell concentrations. Intranasal challenge. Mice were anesthetized with 150 µl of ketamine, acepromazine, and xylazine injected intramuscularly. The mice were then challenged by intranasal instillation with 50 µl of *F. tularensis* or *F. novicda* suspended in PBS from 24 h or 18 h grown freshly swabbed plate cultures, respectively. For all challenge experiments, mice were monitored several times each day and mortality rates (or euthanasia when moribund) were recorded. Aerosol challenge. For aerosol challenges, a 24 hr swabbed plate was used to inoculate flasks containing 25 ml of BHI broth containing 1% Isovitalex at an approximate OD_{600} of 0.025. BHI was chosen as the growth medium for aerosol studies as it was previously shown to be more conducive for *Francisella* survival during aerosolization and improved spray factors (101). The broth cultures were grown overnight at 37^{o}C shaker at 150 rpm. The cultures were adjusted for various challenge doses. Mice were exposed to *F. tularernsis* using a dynamic 30-liter humidity-controlled Plexiglas whole-body exposure chamber, as previously described. The calculated inhaled doses were obtained as previously described (102). *In vivo* dissemination. For *F. tularensis* dissemination studies, mice were challenged intranasally as described above with the indicated strain and dose. At specified time points after challenge, mice were then euthanized within a CO_2 chamber. The lungs and spleens were harvested, rinsed with PBS, weighed, and then homogenized in 1 ml of PBS in a tissue grinder (Kendall Healthcare Precision Disposable Tissue Grinder Systems, Covidien; Mansfield, MA). The homogenates were then serially diluted and plated on to Remel™ chocolate agar plates.

Ethics Statement. Challenged mice were observed at least twice daily for 21 days for clinical signs of illness. Humane endpoints were used during all studies, and mice were humanely euthanized when moribund according to an endpoint score sheet. Animals were

scored on a scale of 0-12: 0-3= no clinical signs; 4-7=clinical signs; increase monitoring; 8-12= distress; euthanize. Those animals receiving a score of 8-12 were humanely euthanized by CO_2 exposure using compressed CO_2 gas followed by cervical dislocation. However, even with multiple checks per day, some animals died as a direct result of the infection.

Animal research at The United States Army of Medical Research Institute of Infectious Diseases was conducted and approved under an Institutional Animal Care and Use Committee in compliance with the Animal Welfare Act, PHS Policy, and other Federal statutes and regulations relating to animals and experiments involving animals. The facility where this research was conducted is accredited by the Association for Assessment and Accreditation of Laboratory Animal Care, International and adheres to principles stated in the Guide for the Care and Use of Laboratory Animals, National Research Council, 2011.

Pathology. Postmortem tissues were collected from mice challenged with *F. tularensis* or *F. novicida*, fixed in 10% neutral buffered formalin, routinely processed, embedded in paraffin, and sectioned for hematoxylin and eosin (HE) staining.

Statistics. For comparing data from the sensitivity to inhibitor and CFU recovery from macrophages, statistical significance ($P< 0.05$) was determined by the two-tailed Student *t* test. Growth of bacterial strains in broth media was analyzed as previously described (103). We used a logistic growth equation to fit the data as a function of maximum density, lag time, and maximum growth rate. LD_{50} analysis was determined by the Bayesian probit analysis. Survival rates were compared between groups by Fisher exact tests with permutation adjustment for multiple comparisons using SAS Version 8.2 (SAS Institute Inc., SAS OnlineDoc, Version 8, Cary, N.C. 2000).

Acknowledgements & Disclaimers:

The authors thank David Fetterer for performing the statistical analysis; Kiley Duncan, Kyle Fitts, and Joshua Roan with assistance with the macrophage assays; and Lorraine Farinick with preparation of the figures. The *Francisella* targeting vector pKEK1140 was generously provided by Karl Klose, University of Texas at San Antonio, San Antonio, TX. The shuttle vector plasmid pMP831 was generously provided by Martin S. Pavelka Jr, University of Rochester Medical Center, Rochester, NY. The monoclonal antibody 11B7 was generously provided by Michael Apicella, University of Iowa, Iowa City, IA.

Opinions, interpretations, conclusions, and recommendations are those of the authors and are not necessarily endorsed by the U.S. Army.

Financial Disclosure

The research described herein was sponsored by the Defense Threat Reduction Agency JSTO-CBD (project number 923698). The funders had no role in study design, data collection and analysis, decision to publish, or preparation of the manuscript

References:

1. McCaffrey RL, Allen LA. Francisella tularensis LVS evades killing by human neutrophils via inhibition of the respiratory burst and phagosome escape. Journal of leukocyte biology. 2006;80(6):1224-30.
2. Hall JD, Craven RR, Fuller JR, Pickles RJ, Kawula TH. Francisella tularensis replicates within alveolar type II epithelial cells in vitro and in vivo following inhalation. Infect Immun. 2007;75(2):1034-9.
3. Clemens DL, Horwitz MA. Uptake and intracellular fate of Francisella tularensis in human macrophages. Ann N Y Acad Sci. 2007;1105:160-86.
4. Lindemann SR, McLendon MK, Apicella MA, Jones BD. An in vitro model system used to study adherence and invasion of Francisella tularensis live vaccine strain in nonphagocytic cells. Infect Immun. 2007;75(6):3178-82.
5. Craven RR, Hall JD, Fuller JR, Taft-Benz S, Kawula TH. Francisella tularensis invasion of lung epithelial cells. Infect Immun. 2008;76(7):2833-42.

6. Anthony LD, Burke RD, Nano FE. Growth of Francisella spp. in rodent macrophages. Infect Immun. 1991;59(9):3291-6.
7. Bolger CE, Forestal CA, Italo JK, Benach JL, Furie MB. The live vaccine strain of Francisella tularensis replicates in human and murine macrophages but induces only the human cells to secrete proinflammatory cytokines. Journal of leukocyte biology. 2005;77(6):893-7.
8. Bosio CM, Dow SW. Francisella tularensis induces aberrant activation of pulmonary dendritic cells. Journal of immunology. 2005;175(10):6792-801.
9. Nutter JE, Myrvik QN. In vitro interactions between rabbit alveolar macrophages and Pasteurella tularensis. Journal of bacteriology. 1966;92(3):645-51.
10. Roberts LM, Tuladhar S, Steele SP, Riebe KJ, Chen CJ, Cumming RI, et al. Identification of early interactions between Francisella and the host. Infect Immun. 2014;82(6):2504-10.
11. Bar-Haim E, Gat O, Markel G, Cohen H, Shafferman A, Velan B. Interrelationship between dendritic cell trafficking and Francisella tularensis dissemination following airway infection. PLoS pathogens. 2008;4(11):e1000211.
12. Jellison WL. Tularemia; geographical distribution of deerfly fever and the biting fly, Chrysops discalis Williston. Public health reports. 1950;65(41):1321-9.
13. Ellis J, Oyston PC, Green M, Titball RW. Tularemia. Clinical microbiology reviews. 2002;15(4):631-46.
14. Markowitz LE, Hynes NA, de la Cruz P, Campos E, Barbaree JM, Plikaytis BD, et al. Tick-borne tularemia. An outbreak of lymphadenopathy in children. JAMA. 1985;254(20):2922-5.
15. Goethert HK, Shani I, Telford SR, 3rd. Genotypic diversity of Francisella tularensis infecting Dermacentor variabilis ticks on Martha's Vineyard, Massachusetts. Journal of clinical microbiology. 2004;42(11):4968-73.
16. Dennis DT, Inglesby TV, Henderson DA, Bartlett JG, Ascher MS, Eitzen E, et al. Tularemia as a biological weapon: medical and public health management. JAMA. 2001;285(21):2763-73.
17. Evans ME, Gregory DW, Schaffner W, McGee ZA. Tularemia: a 30-year experience with 88 cases. Medicine. 1985;64(4):251-69.
18. Saslaw S, Eigelsbach HT, Prior JA, Wilson HE, Carhart S. Tularemia vaccine study. II. Respiratory challenge. Arch Intern Med. 1961;107:702-14.
19. Fritz DL, England MJ, Miller L, Waag DM. Mouse models of aerosol-acquired tularemia caused by Francisella tularensis types A and B. Comparative medicine. 2014;64(5):341-50.
20. Heine HS, Chuvala L, Riggins R, Cirz R, Cass R, Louie A, et al. Natural History of Francisella tularensis in Aerosol-Challenged BALB/c Mice. Antimicrobial agents and chemotherapy. 2016;60(3):1834-40.
21. Twenhafel NA, Alves DA, Purcell BK. Pathology of inhalational Francisella tularensis spp. tularensis SCHU S4 infection in African green monkeys (Chlorocebus aethiops). Veterinary pathology. 2009;46(4):698-706.
22. Saslaw S, Eigelsbach HT, Wilson HE, Prior JA, Carhart S. Tularemia vaccine study. I. Intracutaneous challenge. Arch Intern Med. 1961;107:689-701.
23. Harris S. Japanese biological warfare research on humans: a case study of microbiology and ethics. Ann N Y Acad Sci. 1992;666:21-52.
24. Loveless BM, Yermakova A, Christensen DR, Kondig JP, Heine HS, 3rd, Wasieloski LP, et al. Identification of ciprofloxacin resistance by SimpleProbe, High Resolution Melt and Pyrosequencing nucleic acid analysis in biothreat agents: Bacillus anthracis, Yersinia pestis and Francisella tularensis. Molecular and cellular probes. 2010;24(3):154-60.
25. Sutera V, Levert M, Burmeister WP, Schneider D, Maurin M. Evolution toward high-level fluoroquinolone resistance in Francisella species. The Journal of antimicrobial chemotherapy. 2014;69(1):101-10.

860 26. Gestin B, Valade E, Thibault F, Schneider D, Maurin M. Phenotypic and genetic characterization
861 of macrolide resistance in Francisella tularensis subsp. holarctica biovar I. The Journal of antimicrobial
862 chemotherapy. 2010;65(11):2359-67.
863 27. Kanistanon D, Hajjar AM, Pelletier MR, Gallagher LA, Kalhorn T, Shaffer SA, et al. A Francisella
864 mutant in lipid A carbohydrate modification elicits protective immunity. PLoS pathogens. 2008;4(2):e24.
865 28. Sandstrom G, Sjostedt A, Johansson T, Kuoppa K, Williams JC. Immunogenicity and toxicity of
866 lipopolysaccharide from Francisella tularensis LVS. FEMS microbiology immunology. 1992;5(4):201-10.
867 29. Wang X, Ribeiro AA, Guan Z, Abraham SN, Raetz CR. Attenuated virulence of a Francisella
868 mutant lacking the lipid A 4'-phosphatase. Proceedings of the National Academy of Sciences of the
869 United States of America. 2007;104(10):4136-41.
870 30. Wang X, Ribeiro AA, Guan Z, McGrath SC, Cotter RJ, Raetz CR. Structure and biosynthesis of free
871 lipid A molecules that replace lipopolysaccharide in Francisella tularensis subsp. novicida. Biochemistry.
872 2006;45(48):14427-40.
873 31. Weiss DS, Brotcke A, Henry T, Margolis JJ, Chan K, Monack DM. In vivo negative selection screen
874 identifies genes required for Francisella virulence. Proceedings of the National Academy of Sciences of
875 the United States of America. 2007;104(14):6037-42.
876 32. Gunn JS, Ernst RK. The structure and function of Francisella lipopolysaccharide. Ann N Y Acad Sci.
877 2007;1105:202-18.
878 33. Hajjar AM, Harvey MD, Shaffer SA, Goodlett DR, Sjostedt A, Edebro H, et al. Lack of in vitro and
879 in vivo recognition of Francisella tularensis subspecies lipopolysaccharide by Toll-like receptors. Infect
880 Immun. 2006;74(12):6730-8.
881 34. Fulop M, Webber T, Manchee R. Activation of the complement system by Francisella tularensis
882 lipopolysaccharide. The new microbiologica. 1993;16(2):141-7.
883 35. Ancuta P, Pedron T, Girard R, Sandstrom G, Chaby R. Inability of the Francisella tularensis
884 lipopolysaccharide to mimic or to antagonize the induction of cell activation by endotoxins. Infect
885 Immun. 1996;64(6):2041-6.
886 36. Raetz CR. Biochemistry of endotoxins. Annual review of biochemistry. 1990;59:129-70.
887 37. Phillips NJ, Schilling B, McLendon MK, Apicella MA, Gibson BW. Novel modification of lipid A of
888 Francisella tularensis. Infect Immun. 2004;72(9):5340-8.
889 38. Vinogradov E, Perry MB, Conlan JW. Structural analysis of Francisella tularensis
890 lipopolysaccharide. European journal of biochemistry / FEBS. 2002;269(24):6112-8.
891 39. Kanistanon D, Powell DA, Hajjar AM, Pelletier MR, Cohen IE, Way SS, et al. Role of Francisella
892 lipid A phosphate modification in virulence and long-term protective immune responses. Infect Immun.
893 2012;80(3):943-51.
894 40. Llewellyn AC, Zhao J, Song F, Parvathareddy J, Xu Q, Napier BA, et al. NaxD is a deacetylase
895 required for lipid A modification and Francisella pathogenesis. Molecular microbiology. 2012;86(3):611-
896 27.
897 41. Enderlin G, Morales L, Jacobs RF, Cross JT. Streptomycin and alternative agents for the
898 treatment of tularemia: review of the literature. Clinical infectious diseases : an official publication of
899 the Infectious Diseases Society of America. 1994;19(1):42-7.
900 42. Sawyer WD, Dangerfield HG, Hogge AL, Crozier D. Antibiotic prophylaxis and therapy of airborne
901 tularemia. Bacteriological reviews. 1966;30(3):542-50.
902 43. Overholt EL, Tigertt WD, Kadull PJ, Ward MK, Charkes ND, Rene RM, et al. An analysis of forty-
903 two cases of laboratory-acquired tularemia. Treatment with broad spectrum antibiotics. The American
904 journal of medicine. 1961;30:785-806.
905 44. Hepburn MJ, Simpson AJ. Tularemia: current diagnosis and treatment options. Expert review of
906 anti-infective therapy. 2008;6(2):231-40.

907 45. Cieslak T CG. Medical management of potential biological casualties: a stepwise approach. In: ZF
908 D, editor. Medical aspects of biological warfare. Falls Church, VA; Washington, DC: Office of the Surgeon
909 General, United States Army: Borden Institute, Walter Reed Army Medical Center; 2007. p. 453.
910 46. Scheel O, Reiersen R, Hoel T. Treatment of tularemia with ciprofloxacin. European journal of
911 clinical microbiology & infectious diseases : official publication of the European Society of Clinical
912 Microbiology. 1992;11(5):447-8.
913 47. Johansson A, Berglund L, Gothefors L, Sjostedt A, Tarnvik A. Ciprofloxacin for treatment of
914 tularemia in children. The Pediatric infectious disease journal. 2000;19(5):449-53.
915 48. Arav-Boger R. Cat-bite tularemia in a seventeen-year-old girl treated with ciprofloxacin. The
916 Pediatric infectious disease journal. 2000;19(6):583-4.
917 49. Limaye AP, Hooper CJ. Treatment of tularemia with fluoroquinolones: two cases and review.
918 Clinical infectious diseases : an official publication of the Infectious Diseases Society of America.
919 1999;29(4):922-4.
920 50. Perez-Castrillon JL, Bachiller-Luque P, Martin-Luquero M, Mena-Martin FJ, Herreros V. Tularemia
921 epidemic in northwestern Spain: clinical description and therapeutic response. Clinical infectious
922 diseases : an official publication of the Infectious Diseases Society of America. 2001;33(4):573-6.
923 51. Johansson A, Berglund L, Sjostedt A, Tarnvik A. Ciprofloxacin for treatment of tularemia. Clinical
924 infectious diseases : an official publication of the Infectious Diseases Society of America. 2001;33(2):267-
925 8.
926 52. Sutera V, Caspar Y, Boisset S, Maurin M. A new dye uptake assay to test the activity of
927 antibiotics against intracellular Francisella tularensis. Frontiers in cellular and infection microbiology.
928 2014;4:36.
929 53. Syrjala H, Schildt R, Raisainen S. In vitro susceptibility of Francisella tularensis to
930 fluoroquinolones and treatment of tularemia with norfloxacin and ciprofloxacin. European journal of
931 clinical microbiology & infectious diseases : official publication of the European Society of Clinical
932 Microbiology. 1991;10(2):68-70.
933 54. Berger JM. Type II DNA topoisomerases. Current opinion in structural biology. 1998;8(1):26-32.
934 55. Leo E, Gould KA, Pan XS, Capranico G, Sanderson MR, Palumbo M, et al. Novel symmetric and
935 asymmetric DNA scission determinants for Streptococcus pneumoniae topoisomerase IV and gyrase are
936 clustered at the DNA breakage site. The Journal of biological chemistry. 2005;280(14):14252-63.
937 56. Hooper DC. Mechanisms of action of antimicrobials: focus on fluoroquinolones. Clinical
938 infectious diseases : an official publication of the Infectious Diseases Society of America. 2001;32 Suppl
939 1:S9-S15.
940 57. Hooper DC, Wolfson JS, Ng EY, Swartz MN. Mechanisms of action of and resistance to
941 ciprofloxacin. The American journal of medicine. 1987;82(4A):12-20.
942 58. Wolfson JS, Hooper DC. Fluoroquinolone antimicrobial agents. Clinical microbiology reviews.
943 1989;2(4):378-424.
944 59. Eaves DJ, Randall L, Gray DT, Buckley A, Woodward MJ, White AP, et al. Prevalence of mutations
945 within the quinolone resistance-determining region of gyrA, gyrB, parC, and parE and association with
946 antibiotic resistance in quinolone-resistant Salmonella enterica. Antimicrobial agents and
947 chemotherapy. 2004;48(10):4012-5.
948 60. Meredith TC, Woodard RW. Escherichia coli YrbH is a D-arabinose 5-phosphate isomerase. The
949 Journal of biological chemistry. 2003;278(35):32771-7.
950 61. Apicella MA, Post DM, Fowler AC, Jones BD, Rasmussen JA, Hunt JR, et al. Identification,
951 characterization and immunogenicity of an O-antigen capsular polysaccharide of Francisella tularensis.
952 PLoS One. 2010;5(7):e11060.
953 62. Jones BD, Faron M, Rasmussen JA, Fletcher JR. Uncovering the components of the Francisella
954 tularensis virulence stealth strategy. Frontiers in cellular and infection microbiology. 2014;4:32.

955 63. Rasmussen JA, Fletcher JR, Long ME, Allen LA, Jones BD. Characterization of Francisella
956 tularensis Schu S4 mutants identified from a transposon library screened for O-antigen and capsule
957 deficiencies. Frontiers in microbiology. 2015;6:338.
958 64. Rasmussen JA, Post DM, Gibson BW, Lindemann SR, Apicella MA, Meyerholz DK, et al.
959 Francisella tularensis Schu S4 lipopolysaccharide core sugar and O-antigen mutants are attenuated in a
960 mouse model of tularemia. Infect Immun. 2014;82(4):1523-39.
961 65. Kim TH, Pinkham JT, Heninger SJ, Chalabaev S, Kasper DL. Genetic modification of the O-
962 polysaccharide of Francisella tularensis results in an avirulent live attenuated vaccine. The Journal of
963 infectious diseases. 2012;205(7):1056-65.
964 66. Raynaud C, Meibom KL, Lety MA, Dubail I, Candela T, Frapy E, et al. Role of the wbt locus of
965 Francisella tularensis in lipopolysaccharide O-antigen biogenesis and pathogenicity. Infect Immun.
966 2007;75(1):536-41.
967 67. Nano FE, Zhang N, Cowley SC, Klose KE, Cheung KK, Roberts MJ, et al. A Francisella tularensis
968 pathogenicity island required for intramacrophage growth. Journal of bacteriology. 2004;186(19):6430-
969 6.
970 68. Rodriguez SA, Yu JJ, Davis G, Arulanandam BP, Klose KE. Targeted inactivation of francisella
971 tularensis genes by group II introns. Applied and environmental microbiology. 2008;74(9):2619-26.
972 69. Gallagher LA, Ramage E, Jacobs MA, Kaul R, Brittnacher M, Manoil C. A comprehensive
973 transposon mutant library of Francisella novicida, a bioweapon surrogate. Proceedings of the National
974 Academy of Sciences of the United States of America. 2007;104(3):1009-14.
975 70. Rohmer L, Fong C, Abmayr S, Wasnick M, Larson Freeman TJ, Radey M, et al. Comparison of
976 Francisella tularensis genomes reveals evolutionary events associated with the emergence of human
977 pathogenic strains. Genome biology. 2007;8(6):R102.
978 71. Kilar A, Dornyei A, Kocsis B. Structural characterization of bacterial lipopolysaccharides with
979 mass spectrometry and on- and off-line separation techniques. Mass spectrometry reviews.
980 2013;32(2):90-117.
981 72. Case ED, Chong A, Wehrly TD, Hansen B, Child R, Hwang S, et al. The Francisella O-antigen
982 mediates survival in the macrophage cytosol via autophagy avoidance. Cellular microbiology.
983 2014;16(6):862-77.
984 73. Lindemann SR, Peng K, Long ME, Hunt JR, Apicella MA, Monack DM, et al. Francisella tularensis
985 Schu S4 O-antigen and capsule biosynthesis gene mutants induce early cell death in human
986 macrophages. Infect Immun. 2011;79(2):581-94.
987 74. Conlan JW, Chen W, Shen H, Webb A, KuoLee R. Experimental tularemia in mice challenged by
988 aerosol or intradermally with virulent strains of Francisella tularensis: bacteriologic and histopathologic
989 studies. Microb Pathog. 2003;34(5):239-48.
990 75. Su J, Asare R, Yang J, Nair MK, Mazurkiewicz JE, Abu-Kwaik Y, et al. The capBCA Locus is Required
991 for Intracellular Growth of Francisella tularensis LVS. Frontiers in microbiology. 2011;2:83.
992 76. Su J, Yang J, Zhao D, Kawula TH, Banas JA, Zhang JR. Genome-wide identification of Francisella
993 tularensis virulence determinants. Infect Immun. 2007;75(6):3089-101.
994 77. Twine S, Bystrom M, Chen W, Forsman M, Golovliov I, Johansson A, et al. A mutant of Francisella
995 tularensis strain SCHU S4 lacking the ability to express a 58-kilodalton protein is attenuated for virulence
996 and is an effective live vaccine. Infect Immun. 2005;73(12):8345-52.
997 78. Salomonsson E, Kuoppa K, Forslund AL, Zingmark C, Golovliov I, Sjostedt A, et al. Reintroduction
998 of two deleted virulence loci restores full virulence to the live vaccine strain of Francisella tularensis.
999 Infect Immun. 2009;77(8):3424-31.
1000 79. Wen L, Chmielowski JN, Bohn KC, Huang JK, Timsina YN, Kodali P, et al. Functional expression of
1001 Francisella tularensis FabH and FabI, potential antibacterial targets. Protein expression and purification.
1002 2009;65(1):83-91.

80. Parsons JB, Rock CO. Bacterial lipids: metabolism and membrane homeostasis. Progress in lipid research. 2013;52(3):249-76.
81. Huntley JF, Conley PG, Hagman KE, Norgard MV. Characterization of Francisella tularensis outer membrane proteins. Journal of bacteriology. 2007;189(2):561-74.
82. Wehrly TD, Chong A, Virtaneva K, Sturdevant DE, Child R, Edwards JA, et al. Intracellular biology and virulence determinants of Francisella tularensis revealed by transcriptional profiling inside macrophages. Cellular microbiology. 2009;11(7):1128-50.
83. Thomas RM, Titball RW, Oyston PC, Griffin K, Waters E, Hitchen PG, et al. The immunologically distinct O antigens from Francisella tularensis subspecies tularensis and Francisella novicida are both virulence determinants and protective antigens. Infect Immun. 2007;75(1):371-8.
84. Maier TM, Casey MS, Becker RH, Dorsey CW, Glass EM, Maltsev N, et al. Identification of Francisella tularensis Himar1-based transposon mutants defective for replication in macrophages. Infect Immun. 2007;75(11):5376-89.
85. Li J, Ryder C, Mandal M, Ahmed F, Azadi P, Snyder DS, et al. Attenuation and protective efficacy of an O-antigen-deficient mutant of Francisella tularensis LVS. Microbiology. 2007;153(Pt 9):3141-53.
86. Okan NA, Chalabaev S, Kim TH, Fink A, Ross RA, Kasper DL. Kdo hydrolase is required for Francisella tularensis virulence and evasion of TLR2-mediated innate immunity. mBio. 2013;4(1):e00638-12.
87. Sebastian S, Dillon ST, Lynch JG, Blalock LT, Balon E, Lee KT, et al. A defined O-antigen polysaccharide mutant of Francisella tularensis live vaccine strain has attenuated virulence while retaining its protective capacity. Infect Immun. 2007;75(5):2591-602.
88. Yep A, Sorenson RJ, Wilson MR, Showalter HD, Larsen SD, Keller PR, et al. Enediol mimics as inhibitors of the D-arabinose 5-phosphate isomerase (KdsD) from Francisella tularensis. Bioorganic & medicinal chemistry letters. 2011;21(9):2679-82.
89. Meredith TC, Woodard RW. Identification of GutQ from Escherichia coli as a D-arabinose 5-phosphate isomerase. Journal of bacteriology. 2005;187(20):6936-42.
90. Gourlay LJ, Sommaruga S, Nardini M, Sperandeo P, Deho G, Polissi A, et al. Probing the active site of the sugar isomerase domain from E. coli arabinose-5-phosphate isomerase via X-ray crystallography. Protein science : a publication of the Protein Society. 2010;19(12):2430-9.
91. Sommaruga S, Gioia LD, Tortora P, Polissi A. Structure prediction and functional analysis of KdsD, an enzyme involved in lipopolysaccharide biosynthesis. Biochemical and biophysical research communications. 2009;388(2):222-7.
92. Chamberlain RE. Evaluation of Live Tularemia Vaccine Prepared in a Chemically Defined Medium. Applied microbiology. 1965;13:232-5.
93. Chin CS, Alexander DH, Marks P, Klammer AA, Drake J, Heiner C, et al. Nonhybrid, finished microbial genome assemblies from long-read SMRT sequencing data. Nature methods. 2013;10(6):563-9.
94. Krumsiek J, Arnold R, Rattei T. Gepard: a rapid and sensitive tool for creating dotplots on genome scale. Bioinformatics. 2007;23(8):1026-8.
95. Tatusova T, DiCuccio M, Badretdin A, Chetvernin V, Ciufo S, Li W. Prokaryotic Genome Annotation Pipeline. . 2013. In: The NCBI Handbook [Internet] [Internet]. Bethesda (MD): : National Center for Biotechnology Information (US); . 2nd.
96. Langmead B, Salzberg SL. Fast gapped-read alignment with Bowtie 2. Nature methods. 2012;9(4):357-9.
97. McKenna A, Hanna M, Banks E, Sivachenko A, Cibulskis K, Kernytsky A, et al. The Genome Analysis Toolkit: a MapReduce framework for analyzing next-generation DNA sequencing data. Genome research. 2010;20(9):1297-303.

1050 98. Cingolani P, Platts A, Wang le L, Coon M, Nguyen T, Wang L, et al. A program for annotating and
1051 predicting the effects of single nucleotide polymorphisms, SnpEff: SNPs in the genome of Drosophila
1052 melanogaster strain w1118; iso-2; iso-3. Fly. 2012;6(2):80-92.
1053 99. LoVullo ED, Sherrill LA, Pavelka MS, Jr. Improved shuttle vectors for Francisella tularensis
1054 genetics. FEMS Microbiol Lett. 2009;291(1):95-102.
1055 100. Zhou P, Altman E, Perry MB, Li J. Study of matrix additives for sensitive analysis of lipid A by
1056 matrix-assisted laser desorption ionization mass spectrometry. Applied and environmental microbiology.
1057 2010;76(11):3437-43.
1058 101. Faith SA, Smith LP, Swatland AS, Reed DS. Growth conditions and environmental factors impact
1059 aerosolization but not virulence of Francisella tularensis infection in mice. Frontiers in cellular and
1060 infection microbiology. 2012;2:126.
1061 102. Hartings JM, Roy CJ. The automated bioaerosol exposure system: preclinical platform
1062 development and a respiratory dosimetry application with nonhuman primates. Journal of
1063 pharmacological and toxicological methods. 2004;49(1):39-55.
1064 103. Zwietering MH, Jongenburger I, Rombouts FM, van 't Riet K. Modeling of the bacterial growth
1065 curve. Applied and environmental microbiology. 1990;56(6):1875-81.

1066

1067

Figure Legends:

Fig. 1. Growth assays. *F. tularensis* (A) or *F. novicida* (B) strains were grown in Chamberlain's Defined medium at 37^{o}C with or without the presence of D-arabinose 5-phosphate (A5P) at a concentration of 400 μM. Growth was monitored by optical density. OD measurements were based upon quadruplicate samples and bars represent standard error of the mean. These data represent at least two separate experiments. The growth of the *F. tularenesis kdsD* or *F. novicida kpsF* mutants were severely altered for growth in Chamberlain's medium. However, the addition of A5P to the medium significantly increases the growth of these strains. In contrast, the presence of A5P did not affect the growth of the *F. tularensis* CipR mutant.

Fig 2. Western analysis of *Francisella* strains. Pellets of the (A) *F. tularensis* strains: Schu S4 (WT), CipR, *kdsD*, and *kdsD* complement (Comp) or (B) *F. novicida* strains: U112 (WT), *kpsF*, and *kpsF* complement (Comp) were lysed. Extracts were run on SDS-PAGE gels at equal concentrations and blotted with various antibodies as indicated: monoclonal antibody to the O-antigen of LPS of *F. tularensis* or *F. novicida*; monoclonal antibody to the O-antigen of the *F. tularensis* capsule; or a polyclonal antibody to GroEL of both *F. tularensis* and *F. novicida*. Molecular masses are indicated on the left in KDa.

A) The LPS and capsule profiles of the CipR and *kdsD* mutants were defective in comparison to the WT strain. However, these profiles were restored for the *kdsD* mutant when complemented with a functional gene on a plasmid. Equal loading of sample material was demonstrated when blotting the extracts with an antibody directed against the GroEL protein.

B) The LPS profile of the *kpsF* mutant was defective in comparison to the U112 parent strain. However, the profile was restored for the *kpsF* mutant when complemented with a functional *kdsD* from *F. tularensis* was provided on a plasmid. Equal loading of sample material

was demonstrated when blotting the extracts with an antibody directed against the GroEL protein.

Fig. 3. Characterization of the *F. tularensis* lipid A structure by MALDI-TOF mass spectrometry. LPS extracts from wild type Schu S4 (A), CipR (B), *kdsD*, (C) and complemented *kdsD* mutant were analyzed by negative ion mode MALDI-TOF mass spectrometry. Monoisotopic mass/charge values of the four most prominent species within each spectrum are reported; these values correspond with the expected molecular weights of *F. tularensis* lipid A and its known variants as previously reported (27).

Fig 4. The interaction of *F. tularensis* CipR and *kdsD* mutants with macrophage-like cells show a decrease in CFU recovery and disruption of the host monolayer. J774A.1 cells were infected with A) Schu4 WT or CipR or B) Schu4 WT, *kdsD* mutant, or complemented *kdsD* mutant (+ *kdsD*) at a MOI of ~100:1. Data depict viable counts following gentamycin protection assays. For the 4 h time point, no difference in CFUs was noted between the mutant strains and the respective parent. However, 24 h post-challenge, the mutant strains showed a significant decrease in recovered CFUs (* P=0.0002 or ** P=<0.001;) as compared to the parent. The *kdsD* mutant was complemented with a functional gene, and an increase in CFUs was observed. Error bars represent standard error of the mean values from the CFU counts of triplicates samples which were plated in duplicate. A representative experiment is shown from triplicate experiments.

Panel C shows coverslips of monolayers of J774A.1 cells infected with *F. tularensis* Schu S4 (WT), CipR, *kdsD*, or complemented *kdsD* mutant (+*kdsD*). Cells were fixed at 24 h

post-infection and then subjected to Wright Giemsa staining. Little or no cell death was seen in cells infected with WT or the complemented mutant, and the monolayers remain intact. In contrast, cells infected with cipR and *kdsD* mutant underwent cell death and have lifted off by 24 h post-infection Bar = 20 µm.

Fig. 5. The interaction of *F. novicida kpsF* mutant with macrophage-like cells showed a decrease in CFU recovery and the host cell monolayer undergoing apoptosis. J774A.1 cells were infected with A) the *F. novicida* U112 parent strain, *kpsF* mutant, or complemented *kpsF* mutant (+ *kpsF*) at a MOI of ~100:1. Data depict viable counts following gentamycin protection assays. For the 4 h time point, no difference in CFUs was noted between the mutant strains and the respective parent. However, 24 h post-challenge, the mutant showed a significant decrease in recovered CFUs (* P=0.0042) as compared to the parent. Error bars represent standard error of the mean values from the CFU counts of triplicates samples which were plated in duplicate. A representative experiment is shown from triplicate experiments.

J774A.1 cells, seeded at the same density on coverslips, were left uninfected or infected with *F. novicida* U112, *kpsF*, or the complemented mutant. B) At 18h post-infection, cells were incubated with Caspase 3/7 and infected J774A.1 cells were counted to determine the percentage of cells fluorescing due to apoptosis. The total number of cells counted for each of the samples was WT infected = 1,596; *kpsF* infected = 621; + *kpsF* infected = 892 cells; and uninfected negative control = 689. C) In addition, images of the cells incubated with Caspase 3/7 green ready probes imaged live and fluorescing (left panel) with an accompanying differential interference contrast (DIC) and merge (middle and right column) images taken to show cell density. Cells infected with *kpsF* mutant show an increase in fluorescent signal in the monolayer

indicating cells destined for cell death, in contrast to uninfected and those infected with WT or + *kpsF*.

Fig. 6. The CipR and *kdsD* mutant strains of *F. tularensis* were severely attenuated in BALB/c mice by intranasal and intradermal challenge. Groups of BALB/c mice were challenged and survival monitored following various tularemia models of infection (intranasal (A, C, E, and G) and intradermal (B, D, and F) injections using the wild-type Schu S4 strain (A and B), CipR mutant (A and D), *kdsD* mutant (E and F), and the complemented *kdsD* mutant strain (G). The calculated LD_{50} values from these experiments are included in Table 6.

Fig. 7. Dissemination studies of mice challenged intranasally with *F. tularensis*. Mice were challenged intranasally with Schu S4 (131 CFU), CipR (1,750 CFU), or *kdsD* (6,000 CFU). At set time points, mice were euthanized, and the lungs and spleens were harvested. The lungs and spleens, as indicated, were homogenized and plated to determine bacterial recovery. For each time point, five mice were assayed, except for day 5 for wild-type challenged mice and Day 28 for the CipR challenged mice due to mice having succumbed to infection. The lines (solid= WT Schu S4, hashed= CipR, and dotted= *kdsD*) are connecting at the geometrical means at the data points of CFU recovery from the respective organs and represent the overall trend during the course of infection.

Fig. 8. Pathology of mice challenged intranasally with *F. tularensis* 5 days post-challenge. The strains used for challenge (Schu S4 WT, CipR, and *kdsD*) and HE stained organ (lung, spleen, and liver) are as indicated. All samples shown are at 5 days post challenge when

the Schu S4 challenged mice were moribund; in contrast, the mutant challenged mice displayed no clinical signs of infection at this time point.

Schu S4 WT, Lung (4x) – multifocal areas of inflammation and necrosis (*); arrow indicates the inset area. Inset (40x) – necrosis admixed with inflammatory cells. Spleen (4x) – coalescing areas of necrosis (*) affecting red pulp and white pulp; arrow indicates the inset area. Inset (40x) – necrosis admixed with inflammatory cells. Liver (4x) – Single focus of necrosis (*); arrow indicates the inset area. Insert (40x) – necrosis with few inflammatory cells.

CipR, Lung (4x) – diffuse coalescing necrotic areas. Inset (40x) – necrosis admixed with inflammatory cells. Spleen (4x) – normal. Liver (4x) – normal.

kdsD, Lung (4x) – few foci of necrosis (*); arrow indicates the inset area. Inset (40x) – necrosis admixed with inflammatory cells extends to the surface of the lung. Spleen (4x) – normal. Liver (4x) – normal.

Fig. 9. The CipR and *kdsD* mutant strains of *F. tularensis* are attenuated in BALB/c mice following small particle aerosol challenge. A control group of mice were sprayed with 33 LD_{50} of the parent Schu S4 strain, and all succumbed or were moribund by Day 5. In contrast, other mice were sprayed with either the CipR strain (receiving the equivalent of 43 wild-type LD_{50}) or the *kdsD* mutant (receiving the equivalent of 100 wild-type LD_{50}) and all survived challenge to Day 21 post spray.

Fig. 10. Pathology of mice challenged by small particle aerosol with *F. tularensis*. The strains used for aerosol challenge (Schu S4 WT, CipR, and *kdsD*) and the HE stained organ (lung, spleen, and liver) are as indicated. The mice challenged with Schu S4 were collected at

Day 5 when all mice had succumbed to infection. The mice challenged with the CipR or *kdsD* mutant survived till the end of the study (Day 21) and displayed no clinical signs of infection. Schu S4 WT: Lung (4x) – multifocal areas of inflammation and necrosis (*); arrow indicates the inset area. Inset (40x) – necrosis admixed with inflammatory cells. Spleen (4x) – diffuse coalescing areas of necrosis (*) affecting red pulp and white pulp. Inset (40x) – necrosis (*) admixed with inflammatory cells; arrow indicates the inset area. Liver (10x) – Single focus of necrosis (*); arrow indicates the inset area. Insert (40x) – necrosis with few inflammatory cells. CipR: Lung (4x) – Diffuse coalescing areas of necrosis (*) with inflammatory cells that extend to the surface of the lung. Spleen (4x) – normal. Liver (10x) – normal. *kdsD*: Lung (4x) – foci of necrosis (*) centered on a large airway. Spleen (4x) – normal. Liver (10x) – normal.

Fig. 11. The *kpsF* mutant of *F. novicida* is highly attenuated by intranasal challenge in BALB/c mice. Groups of BALB/c mice were challenged intranasally with the parent U112 strain of *F. novicida* (A), the *kpsF* mutant (B), or the complemented *kpsF* mutant (C). The calculated LD_{50} values from these experiments are included in Table 6.

Table 1. Bacterial strains and plasmids

	Relevant Characteristics	**Reference/ Source**
E. coli		
NEB Turbo	Cloning strain	NEB
F. tularensis		
Schu S4	Fully virulent Type A strain	USAMRIID collection
CipR (Ft-127)	2 mutations in *gyrA* and a 5 bp deletion in *parE*; ciprofloxacin resistant	(24)
kdsD	*kdsD*::*ltrB*$_{L1}$	This study
kdsD with pMP831+*kdsD*	Complemented *kdsD* mutant strain	This study
F. novicida		
U112 strain	*F. tularensis* subsp. *novicida*	ATCC 15482 (13)
kpsF	*kpsF*::T20 (BEI catalog # NR-6746)	BEI (69)
kpsF with pMP831+*kdsD*	Complemented *kpsF*::T20	This study
MIC analysis strains		
E. coli ATCC 25922	Used as a standard for quality control	ATCC
S. aureus ATCC 29213	Used as a standard for quality control	ATCC
P. aeruginosa ATCC 27853	Used as a standard for quality control	ATCC
Plasmids		
pKEK1140	Targetron plasmid	(68)
pKEK1140-*kdsD*	pKEK1140-tgt *kdsD* gene	This study
pMP831	Complementation plasmid	(99)
pMP831+*kdsD*	Plasmid containing the intact *Ft kdsD*	This study

MIC, minimum inhibitory concentration

Table 2. Genetic alterations identified in the CipR strain of *F. tularensis*

Protein	Gene	Function	Gene Size	Mutation and consequence*
YP_169795	*kdsD*	Isomerization of Ru5P to A5P.	987 bp	Addition of A at 174 bp.
YP_170322.1	*fabH*	3-oxoacyl-ACP synthase	972 bp	C→T at 805 bp. Pro→Ser
YP_169814.2	*capA*	Hypothetical poly-gamma-glutamate system protein	1,576 bp	A→G at 2721 bp. Asp→Gly
YP_170326.1	*fabF*	beta-ketoacyl-acylcarrier-protein synthase II	1,638 bp	A→G at 934 bp. Ser→Gly
YP_169692.1	*Ftt0676*	conserved hypothetical membrane protein	1,260 bp	A→G at 848 bp. Glu→Gly
YP_169915.1	*fupA*	Utilize iron bound to siderophores and for siderophore-independent iron acquisition	1,728 bp	Deletion of G at 105 bp; addition of G at 111 bp. Pro →Leu
YP_170495.1	*FtaG*	Hypothetical/ Surface antigen variable number repeat	2,379 bp	C→T at 1517 bp. Thr→Ile.

Intergenic region	Function	Mutation
FTT_0025c - FTT_0026c	Hypothetical protein & drug resistance transporter, Bcr/CflA subfamily	A→G
glgC - glgA	Glucose-1-phosphate adenylyltransferase & glycogen synthase	Deletion of A
FTT_0517 – prmA	Hypothetical protein & 50S ribosomal protein L11 methyltransferase	Deletion of TTTATATAAGT
FTT_1486c – coaE	Hypothetical protein & dephospho-CoA kinase	Deletion of A

* Bp numbers corresponds to ATG=1.

Table 3. Oligonucleotides used in this study.

Oligonucleotide	Sequence
611|612s-IBS	AAAA**CTCGAG**ATAATTATCCTTAGCATGCCCGCTAGTGCGCCCAGATAGGGTG
611|612s-EBS1d	CAGATTGTACAAATGTGGTGATAACAGATAAGTCCCGCTAAATAACTTACCTTTCTTTGT
611|612s-EBS2	TGAACGCAAGTTTCTAATTTCGATTCATGCTCGATAGAGGAAAGTGTCT
kdsD 5' cloning	*CGGACCG*GATTAATTTGAATATGTTTCAT
kdsD 3' cloning	*CGGACCG*GTTAGGTGATCCTGTAATGCTTA
Kan probe F	TGCATGGTTACTCACCACTGC
Kan probe R	TACAACCTATTAATTTCCCCTCG

Bolded sequence corresponds to *Xho*I restriction enzyme site.

Underlined sequence corresponds *to BsrG*I restriction site.

Italics sequence corresponds to *Rsr*II restriction enzyme site.

Table 4. MIC Analysis

Strain	**Ciprofloxacin (µg/ ml)**
F. tularensis Schu S4	<0.03
F. tularensis CipR	64
F. tularensis kdsD	<0.03
F. novicida U112	<0.03
F. novicida kpsF	<0.03
QC Standards	
E. coli ATCC 25922	<0.03
S. aureus ATCC 29213	0.5
P. aeruginosa ATCC 27853	0.25

Table 5. Susceptibilities of *F. tularensis* and *F. novicida* to hydrophobic agents

Strain	PMB[1] ± SD[2]	Tween 20 ± SD	Triton X ± SD	SDS ± SD
Ft Schu S4	10 ± 0	17.7 ± 2.08	35 ± 0	32.3 ± 2.52
Ft CipR	16.0 ± 2.00*	31.7 ± 2.89*	37.7 ± 2.89	37.3 ± 1.16*
Ft kdsD	14.7 ± 0.58*	24.3 ± 0.58*	39.7 ± 3.22	51.0 ± 0*
Ft kdsD Comp	10 ± 0	16.7 ± 1.15	37.0 ± 1.73	25.0 ± 1.00
Fn U112	17 ± 0	10 ± 0	32 ± 3.00	25 ± 0
Fn kpsF	19.3 ± 1.16	19 ± 0*	30 ± 1.00	28.7 ± 3.51
Fn kpsF Comp	20.7 ± 1.16	10 ± 0	33.3 ± 4.93	25.3 ± 3.51

Sterile paper disks (10 mm in diameter) were saturated in polymyxin B at 10 mg/ ml, Tween 20 at 5%, Triton X-100 at 5%, or SDS at 100 mg/ ml, dried, and placed in triplicate onto separate agar plates. Sensitivity to each agent was assessed by measuring the diameter of the zone of growth inhibition around the disk. The results are in millimeters and the average of the three measurements from each separate disk. Representative data is shown from at least duplicate experiments.

Those inhibitors which displayed significant differences ($P < 0.05$) with the mutants strain as compared to measurements with the respective parent strain are indicated by *.

[1] PMB (polymyxin B)
[2] ± SD (standard deviation)

Table 6. Calculated LD_{50} for the *F. tularensis* and *F. novicida* wild-type and mutant strains

Strain	LD_{50} Intranasal	LD_{50} Intradermal
F. tularensis		
Schu S4	1-2 CFU	1-2 CFU
Cip^R	14,468 CFU	>49,000 CFU
kdsD	>82,000 CFU	>36,000 CFU
kdsD complement	<10 CFU	ND
F. novicida		
U112	<23 CFU	ND
kpsF-Tn	25,119 CFU	ND
kpsF complement	32 CFU	ND

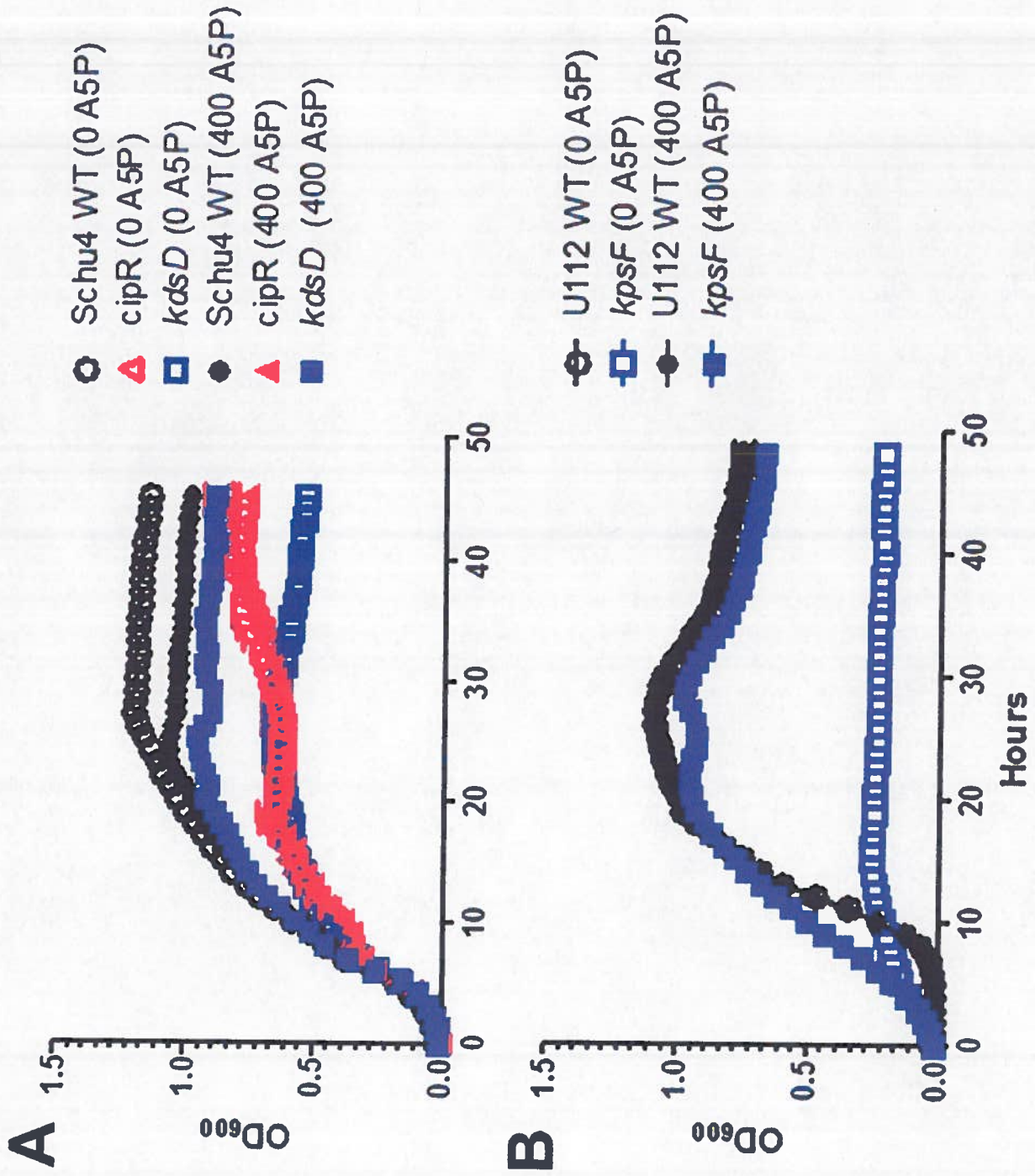
A
B
OD600
Hours
Schu4 WT (0 A5P)
cipR (0 A5P)
kdsD (0 A5P)
Schu4 WT (400 A5P)
cipR (400 A5P)
kdsD (400 A5P)
U112 WT (0 A5P)
kpsF (0 A5P)
U112 WT (400 A5P)
kpsF (400 A5P)
0.0
0.5
1.0
1.5
0
10
20
30
40
50

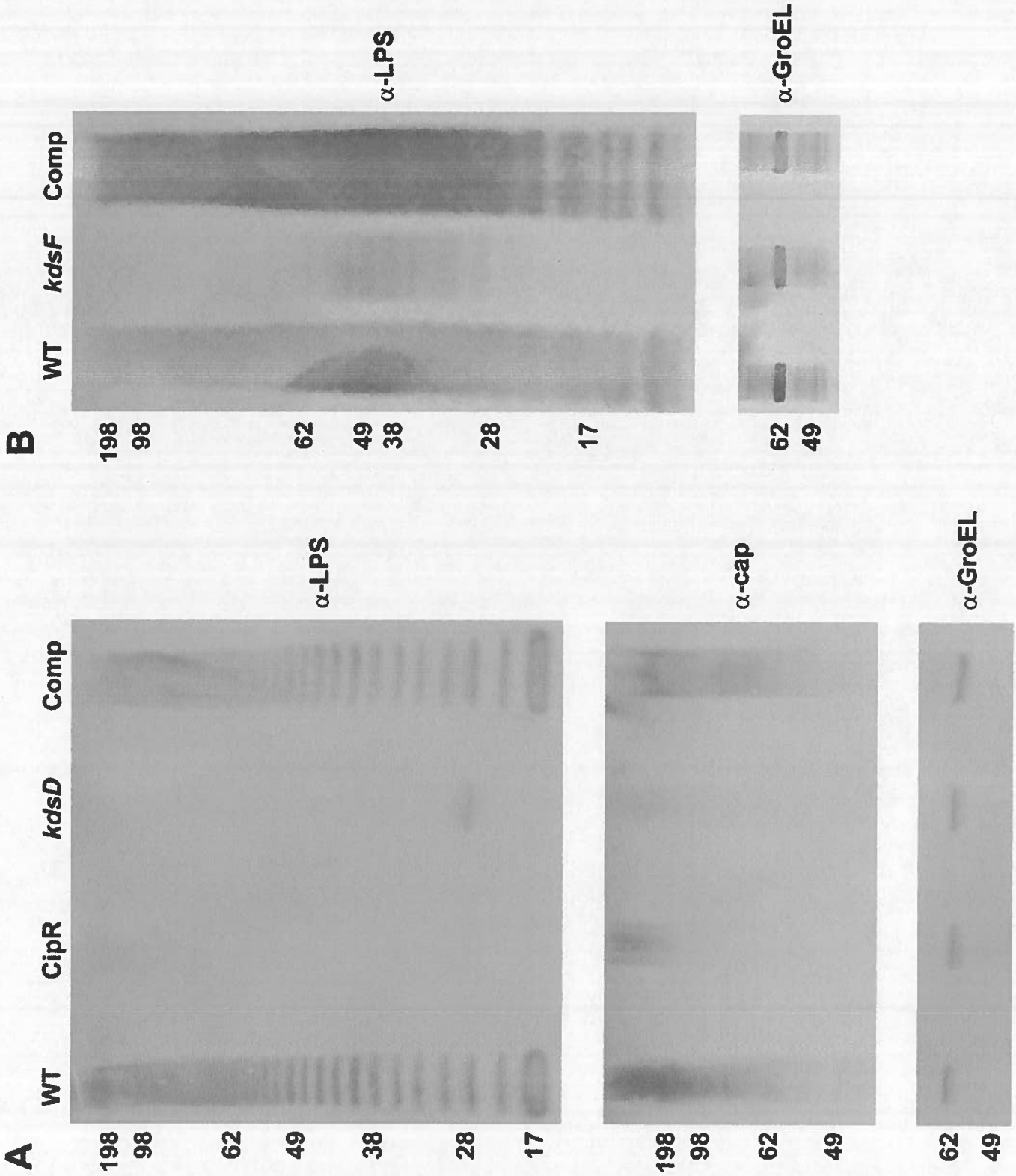
A
WT
CipR
kdsD
Comp
α-LPS
198
98
62
49
38
28
17
α-cap
198
98
62
49
α-GroEL
62
49
B
WT
kdsF
Comp
α-LPS
198
98
62
49
38
28
17
α-GroEL
62
49

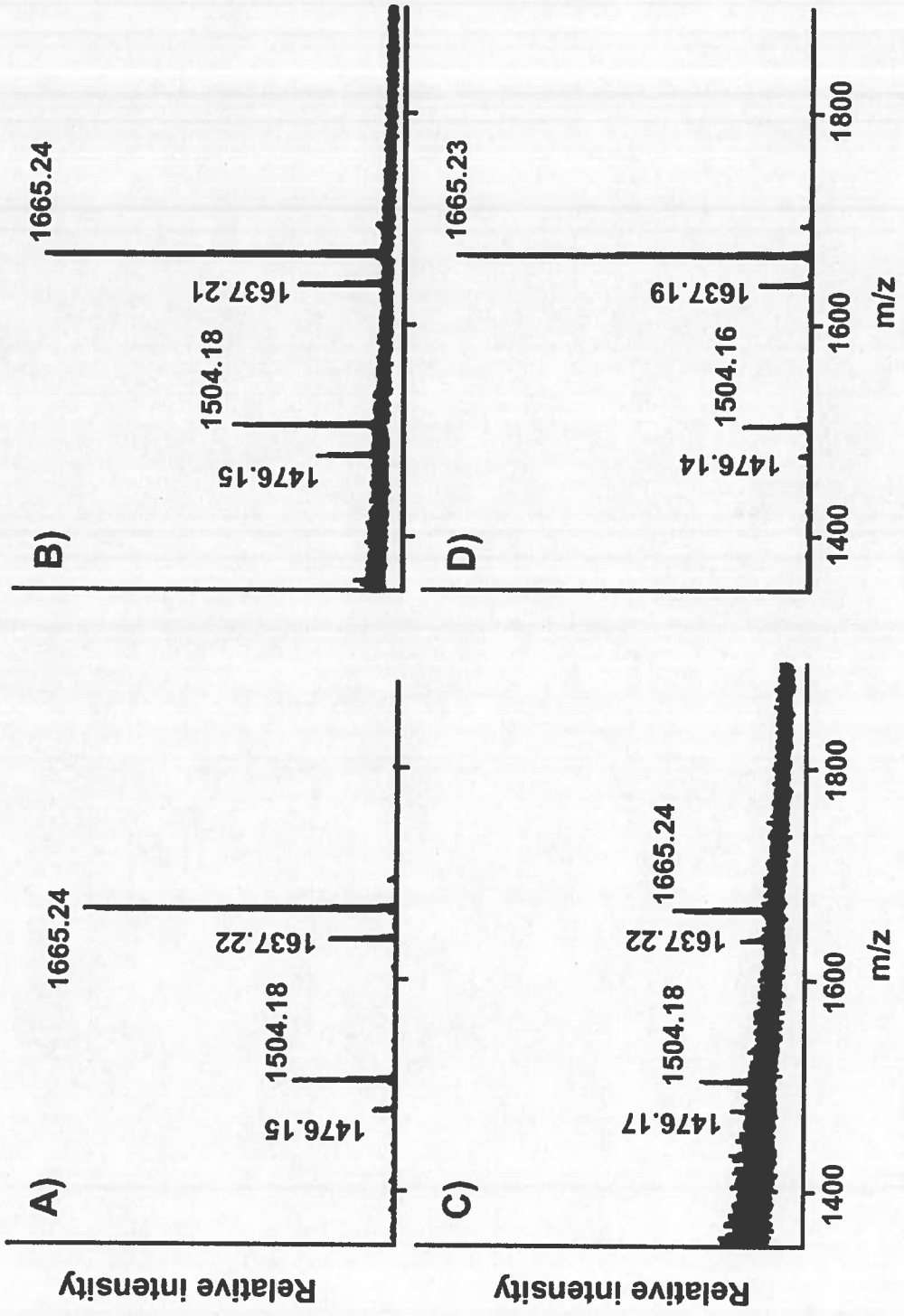
A)
1665.24
1637.22
1504.18
1476.15
B)
1665.24
1637.21
1504.18
1476.15
C)
1665.24
1637.22
1504.18
1476.17
D)
1665.23
1637.19
1504.16
1476.14
Relative intensity
Relative intensity
1400
1600
1800
m/z

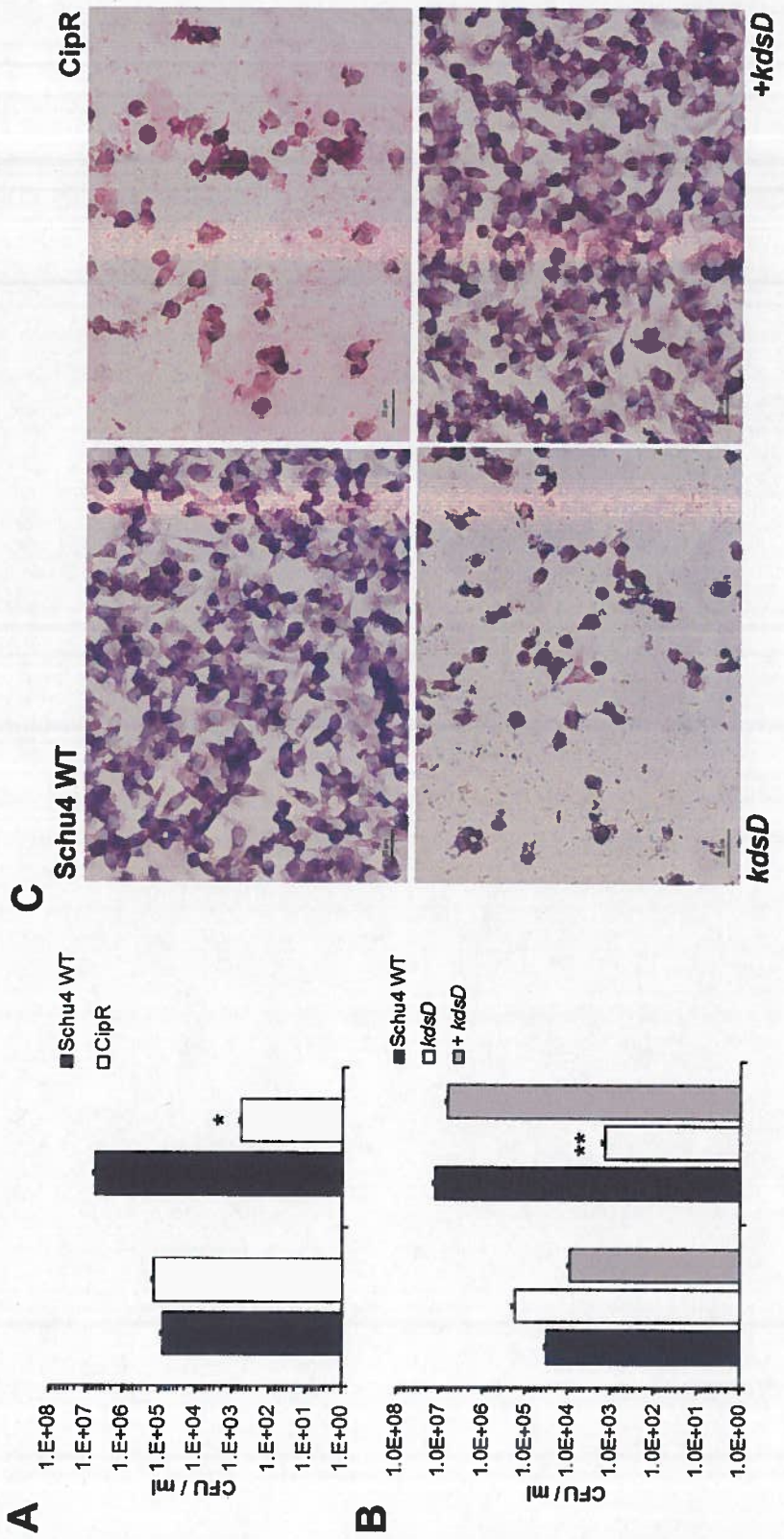
A
Schu4 WT
CipR
CFU / ml
1.E+08
1.E+07
1.E+06
1.E+05
1.E+04
1.E+03
1.E+02
1.E+01
1.E+00
*
B
Schu4 WT
kdsD
+ kdsD
CFU / ml
1.0E+08
1.0E+07
1.0E+06
1.0E+05
1.0E+04
1.0E+03
1.0E+02
1.0E+01
1.0E+00
**
C
Schu4 WT
CipR
kdsD
+kdsD

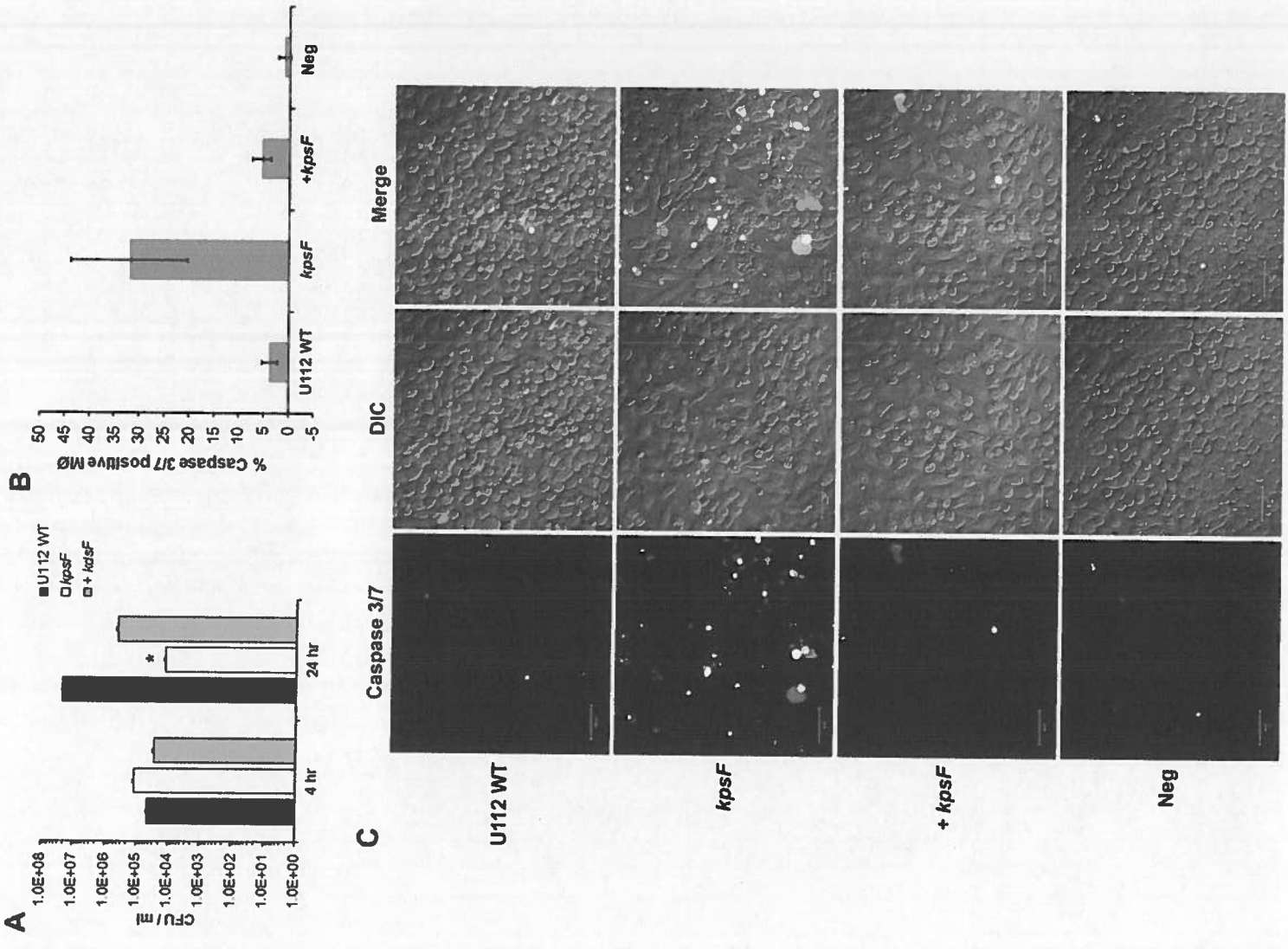
A
CFU / ml
1.0E+08
1.0E+07
1.0E+06
1.0E+05
1.0E+04
1.0E+03
1.0E+02
1.0E+01
1.0E+00
4 hr
24 hr
*
U112 WT
kpsF
+ kdsF
B
% Caspase 3/7 positive MØ
50
45
40
35
30
25
20
15
10
5
0
-5
U112 WT
kpsF
+kpsF
Neg
C
Caspase 3/7
DIC
Merge
U112 WT
kpsF
+ kpsF
Neg

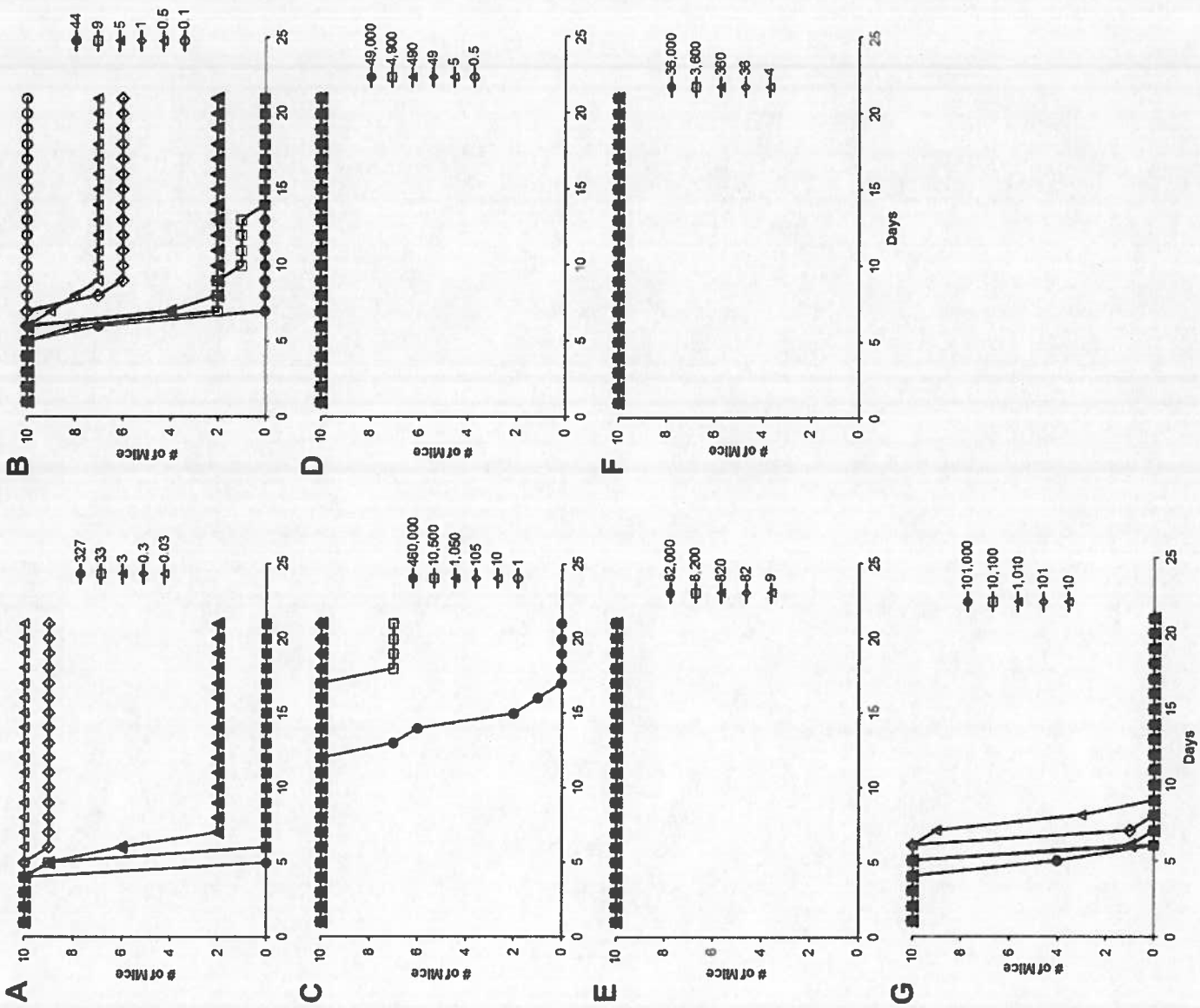
A
B
C
D
E
F
G
# of Mice
Days
327
33
3
0.3
0.03
44
9
5
1
0.5
0.1
480,000
10,500
1,050
105
10
1
49,000
4,900
490
49
5
0.5
82,000
8,200
820
82
9
36,000
3,600
360
36
4
101,000
10,100
1,010
101
10

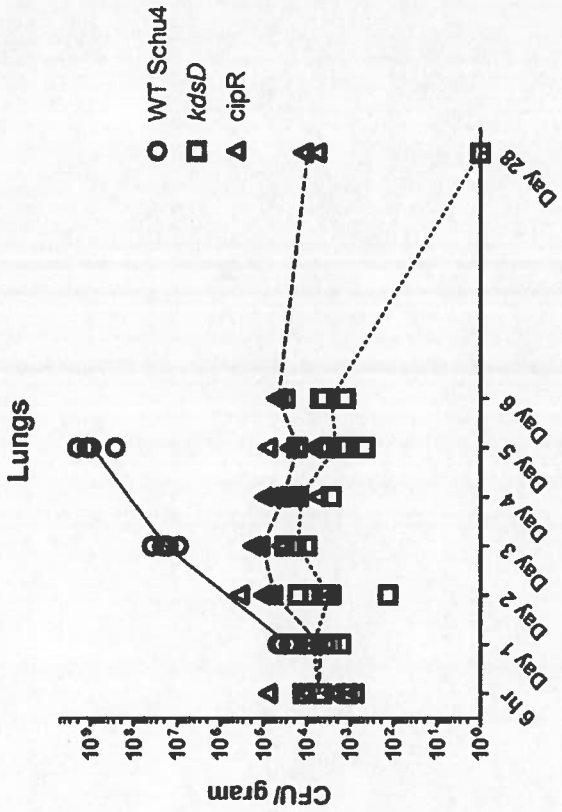
Lungs
WT Schu4
kdsD
cipR
CFU/ gram
6 hr
Day 1
Day 2
Day 3
Day 4
Day 5
Day 6
Day 28

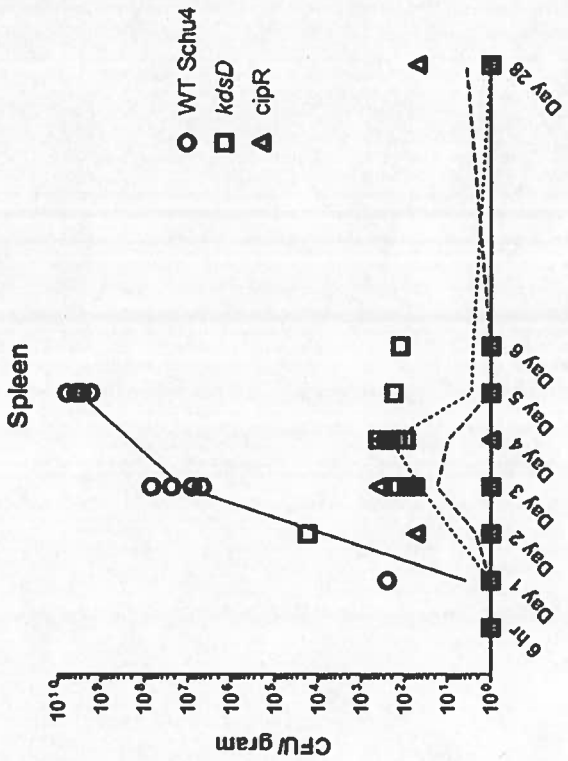
Spleen
WT Schu4
kdsD
cipR
CFU/ gram
6 hr
Day 1
Day 2
Day 3
Day 4
Day 5
Day 6
Day 28

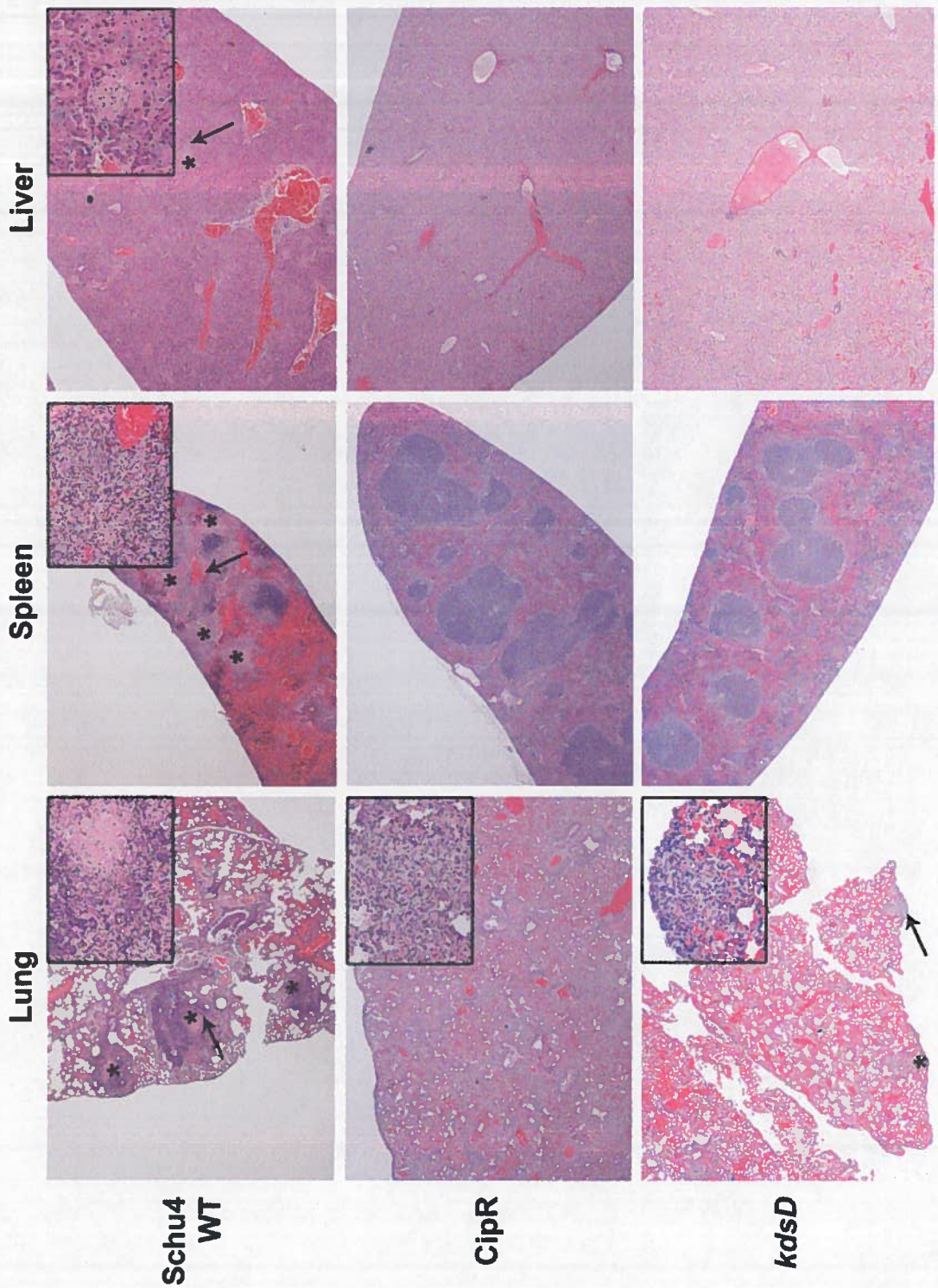
Liver
Spleen
Lung
Schu4 WT
CipR
kdsD

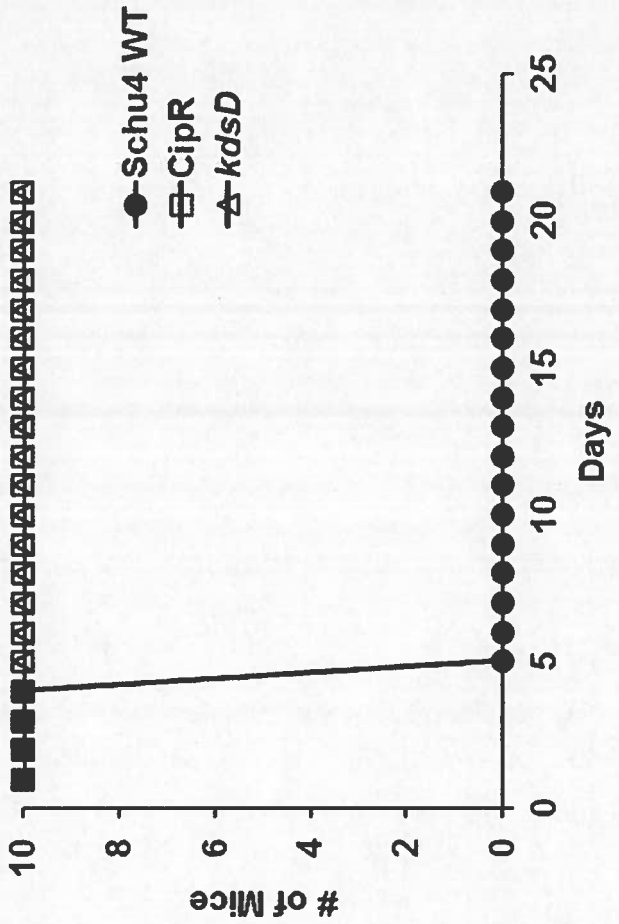
Schu4 WT
CipR
kdsD
# of Mice
0
2
4
6
8
10
0
5
10
15
20
25
Days

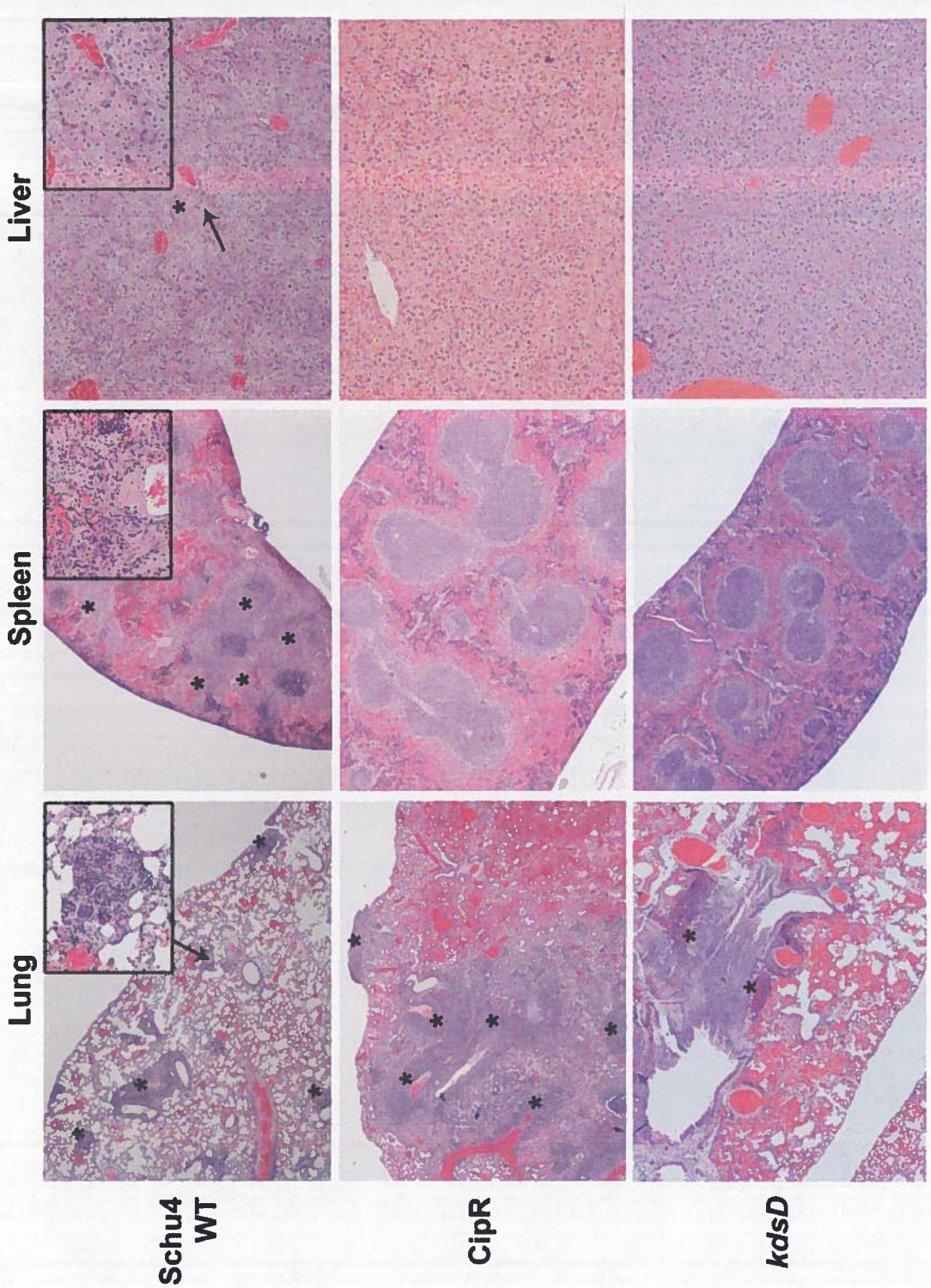
Liver
Spleen
Lung
Schu4 WT
CipR
kdsD

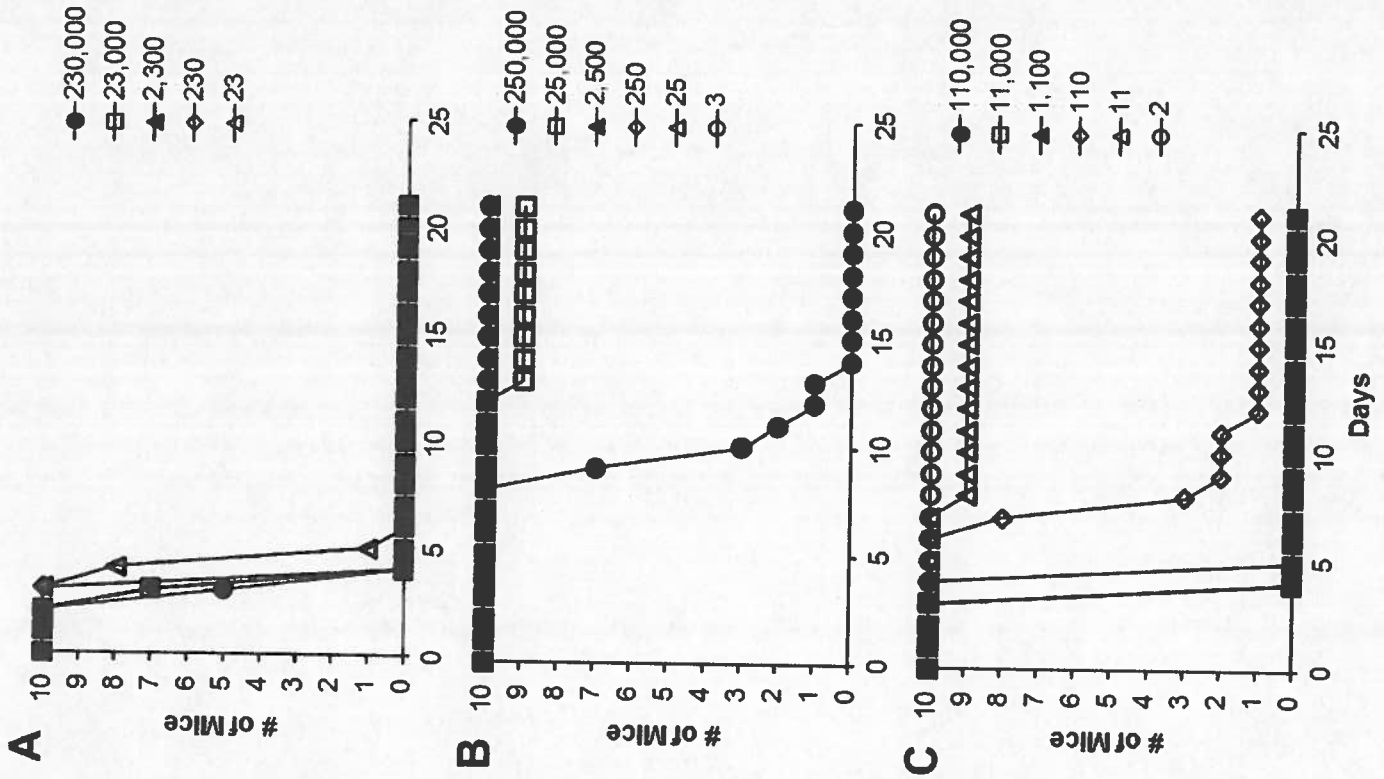
A
B
C
# of Mice
Days
230,000
23,000
2,300
230
23
250,000
25,000
2,500
250
25
3
110,000
11,000
1,100
110
11
2